Dynamical Mountain Meteorology

Dr. Yuh-Lang Lin, ylin@cat.edu; http://mesolab.org
Department of Physics/Department of Energy & Environmental Systems
North Carolina A&T State University
(Ref.: *Mesoscale Dynamics*, Y.-L. Lin, Cambridge, 2007)

Chapter 13 Thermally Forced Flow over Mountains

[Based on Ch. 6 of *Mesoscale Dynamics* (Lin 2007)]

6. Thermally Forced Flows

- Some of the basic dynamics of thermally forced flows can be understood by prescribing diabatic heating or cooling. This approach makes the mathematical problem more tractable.

- These problems include
  - Heat island circulations
  - Sea and land breezes
  - Mountain-plain solenoidal circulations
  - Density current generation and propagation
  - Flow over thunderstorm tops
  - Circulations and gravity waves forced by differential heating
  - Moist convection
  - Orographic precipitation systems.

6.1 Two-dimensional flows

6.1.1 Steady flows over a sinusoidal heat source

- For 2D, steady-state, uniform, constant stratification, nonrotating, inviscid, Boussinesq flow over a two-dimensional mesoscale heat source, (2.2.14) - (2.2.18) reduce to

$$U\frac{\partial u'}{\partial x}+\frac{1}{\rho_o}\frac{\partial p'}{\partial x}=0, \tag{6.1.1}$$

$$U\frac{\partial w'}{\partial x}-g\frac{\theta'}{\theta_o}+\frac{1}{\rho_o}\frac{\partial p'}{\partial z}=0, \tag{6.1.2}$$

$$\frac{\partial u'}{\partial x}+\frac{\partial w'}{\partial z}=0, \text{ and} \tag{6.1.3}$$

$$U\frac{\partial \theta'}{\partial x}+\frac{N^2\theta_o}{g}w'=\frac{\theta_o}{c_pT_o}q'. \tag{6.1.4}$$

The above fluid system is similar to that discussed for orographically forced flow except with thermal forcing.

Eqs. (6.1.1) – (6.1.4) can be combined into a single equation for the vertical velocity:

$$\frac{\partial^2 w'}{\partial x^2}+\frac{\partial^2 w'}{\partial z^2}+l^2w'=\frac{g}{c_pT_oU^2}q', \tag{6.1.5}$$

where $l^2=N^2/U^2$ is the square of the *Scorer parameter*, as defined in (5.1.6), for a uniform basic flow (U_{zz} = 0).

The mathematical approach in solving (6.1.5) is similar to the problem of flow over mountains except having to treat the hermal forcing by using the *Green's function method*.

As a first approximation, we may assume a separable heating function,

$$q'(x,z) = Q_o f(x) g(z), \tag{6.1.6}$$

where $g(z)$ is normalized according to

$$\int_0^\infty g(z)dz = 1, \tag{6.1.7}$$

so that

$$\rho_o \int_0^\infty q'(x,z)dz = \rho_o Q_o f(x), \tag{6.1.8}$$

which represents the total thermal energy added to a vertical column of the atmosphere per unit time.

Note that the net heating involved in diabatic processes in a steady state fluid flow tends to produce a vertical displacement that continues to increase downstream. To avoid the *net heating problem*, we impose the constraint

$$\int_{-\infty}^\infty f(x)dx = 0, \tag{6.1.9}$$

at every level.

We then apply the *Green's function method* by assuming the heating is concentrated at height $z = 0$ in an unbounded atmosphere,

$$q'(x,z) = Q_o f(x)\delta(z=0). \tag{6.1.10}$$

At the interface, $z = 0$, the *kinematic boundary condition* (3.7.11) requires that the vertical velocity be continuous, i.e.

$$w'(z=0^+) = w'(z=0^-), \tag{6.1.11}$$

where $z = 0^+$ and $z = 0^-$ denote the heights just above and below $z = 0$, respectively.

Substituting (6.1.10) into (6.1.5) and integrating it from $z = 0^-$ to $z = 0^+$ gives the second interface condition, i.e. the *dynamic boundary condition* (3.7.13),

$$w'_z(0^+) - w'_z(0^-) = \frac{gQ_o f(x)}{c_p T_o U^2}. \qquad (6.1.12)$$

The above condition is equivalent to the continuity of perturbation pressure across the interface (Ch. 4).

Away from $z = 0$, (6.1.5) reduces to the *Scorer's equation*, i.e. (5.1.5),

$$w'_{xx} + w'_{zz} + l^2 w' = 0. \qquad (6.1.13)$$

The mathematical problem associated with appropriate upper and lower boundary conditions in (6.1.11) - (6.1.13) is similar to problems encountered in mountain wave theory (Sec. 5.1-5.2).

For simplicity, we consider a spatially sinusoidal heating function

$$q'(x,z) = Q_o \cos kx\, \delta(z=0), \qquad (6.1.14)$$

and look for solutions in the form of

$$w'(x,z) = w_1(z)\cos kx + w_2 \sin kx. \qquad (6.1.15)$$

Thus, Scorer's equation, which governs solutions for w_i, i=1, 2, becomes

$$w_{izz} + (l^2 - k^2) w_i = 0, \quad i = 1, 2. \qquad (6.1.16)$$

As in mountain wave theory, two regimes are associated with (6.1.16), namely,

(1) $k^2 > l^2$: the evanescent wave regime, and

(2) $k^2 < l^2$: the vertically propagating wave regime.

For $k^2 > l^2$, the solutions can be written as

$$w_i(x,z) = A_i(x)e^{-\lambda z} + B_i(x)e^{\lambda z}, \quad \text{for } z \geq 0, \qquad (6.1.17a)$$

$$w_i(x,z) = C_i(x)e^{-\lambda z} + D_i(x)e^{\lambda z}, \quad \text{for } z < 0, \qquad (6.1.17b)$$

where $\lambda = \sqrt{k^2 - l^2}$.

Terms B_i and C_i represent disturbances that increase in the vertical away from the heating level, and should be eliminated, i.e, $B_i = C_i = 0$, in order to satisfy the boundedness condition, at infinity far from the energy source located at $z = 0$.

Applying the interface conditions (6.1.11) and (6.1.12) to (6.1.17) leads to

$$w'(x,z) = \left(\frac{-gQ_o}{2c_p T_o U^2} \right) \frac{\cos kx}{\sqrt{k^2 - l^2}} e^{-\sqrt{k^2 - l^2}|z|}, \quad \text{for } k^2 > l^2 . \qquad (6.1.18)$$

As demonstrated in Chapters 3 and 5, the condition $k^2 > l^2$ corresponds to $2\pi / N > L/U$, i.e. a relatively stronger wind with weaker stability over a narrower heat source. When $k^2 >> l^2$, the buoyancy force becomes extremely weak and can be ignored. In this limit, the disturbance will approach a *potential* (*irrotational*) *flow*,

$$w'(x,z) = \left(\frac{-gQ_o}{2c_p T_o U^2 k} \right) \cos kx \, e^{-k|z|} . \qquad (6.1.19)$$

The flow field of the evanescent waves is simply a negative cosine function at the heating level ($z = 0$), that exponentially decays with height away from this level. The negative phase of the vertical motion and heating will be explained later.

When $k^2 < l^2$, the solution for (6.1.16) can be written as

$$w_i(z) = A_i \sin mz + B_i \cos mz , \; i = 1, 2 , \qquad (6.1.20)$$

where $m^2 = l^2 - k^2$. Combining this with (6.1.15), the above solution can be rewritten as

$$w'(x,z) = C\cos(kx + mz) + D\cos(kx - mz) + E\sin(kx + mz) + F\sin(kx - mz) ,$$
$$\text{for } z \geq 0 , \qquad (6.1.21a)$$
$$w'(x,z) = C'\cos(kx + mz) + D'\cos(kx - mz) + E'\sin(kx + mz) + F'\sin(kx - mz) ,$$
$$\text{for } z < 0 , \qquad (6.1.21b)$$

As in mountain wave theory, terms with argument $kx + mz$ have an upstream phase tilt with height and represent upward energy propagation for $z > 0$, while terms with argument

$kx - mz$ have a downstream phase tilt and represent downward energy propagation for $z < 0$.

Since the energy source is located at $z = 0$, the upper and lower radiation conditions require $D = F = C' = E' = 0$. Applying the interface conditions (6.1.11) and (6.1.12) to (6.1.21), we obtain

$$w'(x,z) = \left(\frac{gQ_o}{2c_p T_o U^2} \right) \left(\frac{\sin\left(kx + \sqrt{l^2 - k^2}\,|z| \right)}{\sqrt{l^2 - k^2}} \right), \quad \text{for } k^2 < l^2 \qquad (6.1.22)$$

The above solution represents *vertically propagating waves*, which satisfy the radiation conditions at $z = \pm\infty$. Again, the condition $k^2 < l^2$ corresponds to $2\pi / N < L / U$, i.e. a relatively weaker wind with stronger stability over a broader heat source.

The flow response predicted by (6.1.22) becomes hydrostatic for $k^2 << l^2$. In this limit, the above equation reduces to

$$w'(x,z) = \left(\frac{gQ_o}{2c_p T_o U^2 l} \right) \sin\left(kx + l|z| \right), \qquad (6.1.23)$$

As in mountain wave theory, the above solution at $x = 0$ repeats itself with a vertical wavelength of $2\pi U / N$, which is referred to as the *hydrostatic vertical wavelength*. With a typical atmospheric situation of $U = 10$ ms^{-1} and $N = 0.01$ s^{-1}, the vertical wavelength of the forced wave is about 6.28 km. As is the case in the mountain wave theory, when the vertical displacement (η) is in a steady-state and the flow is linear, η is related to w' through

$$w' = U \frac{\partial \eta}{\partial x}. \qquad (6.1.24)$$

- Figure 6.1 shows an example for an unbounded, hydrostatic, stratified airflow over a periodic heating and

cooling concentrated at the $z = 0$ level.

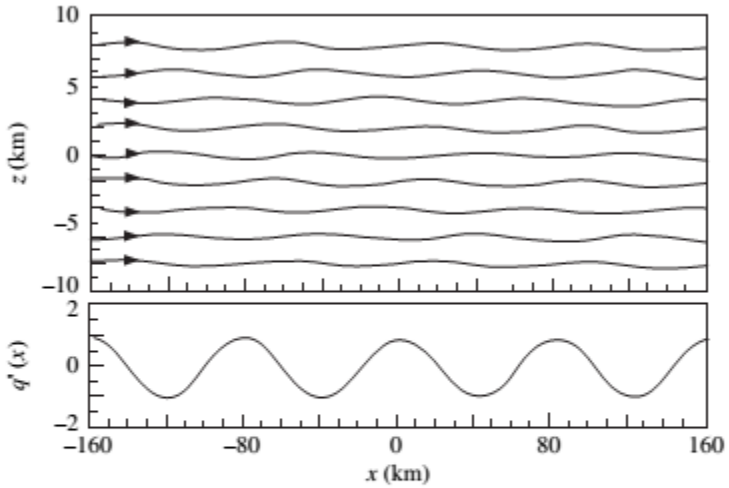

Fig. 6.1 The vertical displacement of an unbounded, hydrostatic stratified airflow for periodic heating and cooling concentrated at the $z = 0$ level, as implied by (6.1.23). The parameters used are: $U = 10\ \mathrm{m\,s^{-1}}$, $N = 0.01\ \mathrm{s^{-1}}$, $L = 2\pi/k = 80\,\mathrm{km}$, $Q_o = 1200\ \mathrm{J\,kg^{-1}\ m\,s^{-1}}$, $T_o = 287\,\mathrm{K}$. The normalized heating rate function, $q'(x, z) = Q_o \cos kx\ \delta(z = 0)$, at $z = 0$ is shown in the lower panel. The unit of q' is $\mathrm{J\,kg^{-1}s^{-1}}$. Vertically propagating waves are evident from the upstream phase tilting above and below the heating level. (From Smith and Lin 1982.)

- Vertically propagating waves are evident above and below the heating level with upstream phase tilting.

- Note that *the vertical displacement at the heating level is exactly out of phase with the heating and cooling* in Fig. 6.1. That is, the air parcel is displaced downward (upward) in the heating (cooling) region.

➢ A similar phenomenon has been observed over heat islands. For example, Fig. 6.2 shows that, during the daytime, there is a downward motion over Barbados followed by an upward motion over the ocean on the downwind side. This is also consistent with other theoretical studies on stratified flow over a diabatic heat source or sink.

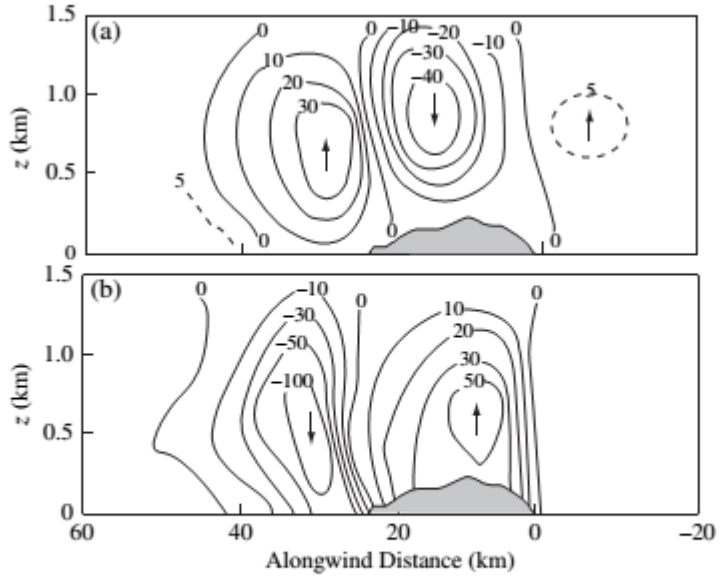

Fig. 6.2 Vertical velocity fields observed over Barbados during the summers of 1968 and 1969 by: (a) the day and (b) the night (DeSouza 1972). The basic wind is from right. The unit of w' is 0.01 m s^{-1}. (Adapted after Garstang *et al.* 1975.)

- The responses to diabatic forcing are closely related to the flow speed or the Froude number associated with thermal forcing.

- Another example is that mountain waves may be strengthened by sensible cooling (Fig. 6.3b) and weakened by sensible heating. Responses to diabatic forcing are closely related to the flow speed or the Froude number associated with thermal forcing which will be discussed in Section 6.2.

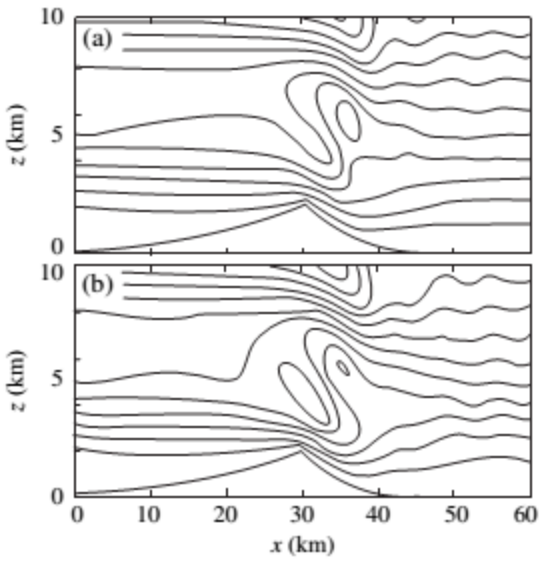

Fig. 6.3 Streamlines for airflow over a mountain ridge: (a) with no sensible heating or cooling (adiabatic), and (b) with boundary layer sensible cooling. Note that the adiabatic mountain waves are strengthened by the sensible cooling. A similar result has also been found in Olfe and Lee (1971). (Adapted after Raymond 1972.)

Similar to (5.1.25), the vertical flux of horizontal momentum can be calculated by

$$\mathcal{D} = \rho_o \int_0^L u'w'\,dx\,, \qquad (6.1.25)$$

where $L\ (=2\pi/k)$ is the horizontal wavelength of the heating. From (6.1.23) and (6.1.25), we have

$$\frac{\mathcal{D}}{L} = \frac{-\rho_o}{2kl}\left(\frac{gQ_o}{2c_pT_oU^2}\right)^2 \frac{z}{|z|}\,. \qquad (6.1.26)$$

The transport of mechanical energy away from the layer of thermal forcing is accompanied by a flux of horizontal momentum towards the layer.

To examine the effect of vertical momentum flux, we consider the time-dependent nonlinear horizontal momentum equation

$$\frac{\partial u'}{\partial t} + U\frac{\partial u'}{\partial x} + \frac{1}{\rho_o}\frac{\partial p'}{\partial x} = -u'\frac{\partial u'}{\partial x} - w'\frac{\partial u'}{\partial z}\,. \qquad (6.1.27)$$

Taking the horizontal integration over one wavelength yields

$$\frac{\partial \bar{u}}{\partial t} = -\frac{\partial}{\partial z}\overline{uw}, \qquad (6.1.28)$$

where

$$\overline{(\quad)} = \frac{1}{L}\int_0^L (\quad) dx. \qquad (6.1.29)$$

Thus, the convergence of the vertical momentum flux tends to accelerate the flow. Note that this acceleration is not explicitly accounted for in linear theory since nonlinear terms are neglected. This acceleration may be relevant to the problems of moist convection, heat islands, and orographic precipitation.

6.1.2 Steady flows over an isolated heat source

A useful localized heating function may be chosen

$$q'(x,z) = Q_o\left(\frac{b_1^2}{x^2+b_1^2} - \frac{b_1 b_2}{x^2+b_2^2}\right)\delta(z-z_H), \qquad (6.1.30)$$

where z_H is the level of thermal forcing, b_1 is the half-width of the heating function and b_2 is the horizontal scale of the compensated cooling.

Substituting the above equation into (6.1.5) leads to

$$w'_{xx} + w'_{zz} + l^2 w' = \left(\frac{gQ_o}{c_p T_o U^2}\right)\left(\frac{b_1^2}{x^2+b_1^2} - \frac{b_1 b_2}{x^2+b_2^2}\right)\delta(z-z_H). \qquad (6.1.31)$$

Details of the solution can be found below.

Applying the one-sided Fourier transform of $w'(x,z)$ in x to (6.1.31) yields (Appendix 5.1),

$$\tilde{w}_{zz} + (l^2 - k^2)\tilde{w} = \left(\frac{gQ_o b_1}{2c_p T_o U^2} \right) \left(e^{-kb_1} - e^{-kb_2} \right) \delta(z - z_H) . \qquad (6.1.32)$$

For $z \neq z_H$, (6.1.32) reduces to the Scorer's equation, (6.1.13), in the Fourier space,

$$\tilde{w}_{zz} + (l^2 - k^2)\tilde{w} = 0 . \qquad (6.1.33)$$

For a hydrostatic wave ($k^2 << l^2$), the solution may be written as

$$\tilde{w}(k,z) = Ae^{ilz} + Be^{-ilz} \quad \text{for } 0 \le z < z_H , \qquad (6.1.34a)$$

$$\tilde{w}(k,z) = Ce^{ilz} + De^{-ilz} \quad \text{for } z_H \le z . \qquad (6.1.34b)$$

The lower boundary condition requires $w' = 0$ over a flat surface at $z = 0$. As in the previous discussion and in the mountain wave theory, the upper radiation boundary condition requires $D = 0$. The interface boundary conditions may be determined in a similar manner to that used for the periodic heat source problem (subsection 5.1.1) using (6.1.11) and (6.1.12). Once the interface boundary conditions have been determined, applying them to (6.1.34), using (6.1.24) and taking the inverse Fourier transform allows us to obtain the vertical displacement for a heating concentrated at $z = z_H$,

$$\eta(x,z) = -A_1 \sin lz \left\{ T_1(x) \cos lz_H + L_1(x) \sin lz_H \right\}, \quad \text{for } 0 \le z < z_H , \qquad (6.1.35a)$$

$$\eta(x,z) = -A_1 \sin lz_H \left\{ T_1(x) \cos lz + L_1(x) \sin lz \right\}, \quad \text{for } z_H \le z , \qquad (6.1.35b)$$

where

$$A_1 = \frac{gQ_o b_1}{c_p T_o U^3 l}, \; T_1(x) = \tan^{-1}\left(\frac{x}{b_1} \right) - \tan^{-1}\left(\frac{x}{b_2} \right), \; L_1(x) = \frac{1}{2} \ln\left(\frac{x^2 + b_2^2}{x^2 + b_1^2} \right).$$

The vertical displacement for heating distributed in a layer can be determined by superposition of the above solution through integration.

The surface pressure perturbation can be calculated from (6.1.35) using *Bernoulli's equation*, which is obtained by substituting (6.1.3) and (6.1.24) into (6.1.1),

$$p'(x,0) = -(\rho_o U^2 l)\, A_1 \{T_1(x)\cos lz_H + L_1(x)\sin lz_H\}. \qquad (6.1.36)$$

The vertical momentum flux associated with (6.1.35) is

$$\mathcal{D} = 0, \qquad \text{for } 0 \le z < z_H, \qquad (6.1.37a)$$

$$\mathcal{D} = -\pi\rho_o U A_1 \ln\{(b_1+b_2)^2/4b_1b_2\}, \qquad \text{for } z_H \le z, \qquad (6.1.37b)$$

The vertical displacement and surface pressure perturbation produced by the thermally induced gravity waves satisfy the rigid lower boundary condition $w' = 0$ at $z = 0$, thus causing complete reflection of the downward propagating wave produced by the elevated heating. Flux cancellation of the upward and downward propagating waves results in a vertical momentum flux of zero between the heating level and the surface. This gives the disturbance no vertical phase tilt.

- The flow response is sensitive to the heating level since the upward propagating and downward propagating waves may cancel each other out. If the heating is added very near the surface, $lz_H << 1$, the resulting disturbance is extremely small and may be neglected. From (6.1.35), cancellation of the direct upward propagating wave and the reflected upward propagating wave above z_H can also occur at $lz_H = 0, \pi, 2\pi, ..., n\pi$. This effect is less evident if the heating is spread over a layer of finite depth.

- Figure 6.4 shows an example of the hydrostatic response to isolated heating and widespread cooling [(6.1.30)] added at $lz_H = \pi/2$.

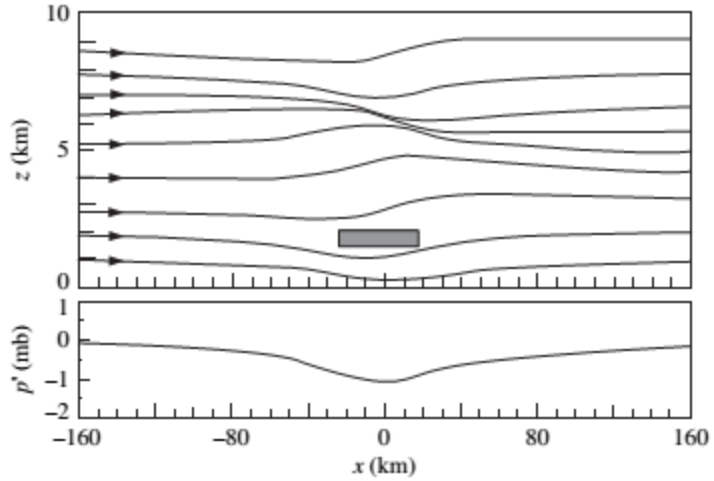

Fig. 6.4 Hydrostatic response of a stratified airstream to an isolated heating-widespread cooling function (6.1.30) with $Q_o = 900$ W m kg^{-1}, $b_1 = 20$ km, $b_2 = 100$ km, $U = 10$ m s^{-1} and $N = 0.01$ s^{-1}: (a) vertical displacement and (b) perturbation pressure. The lower surface is flat. A low pressure is generated directly below the region of concentrated heating (shaded). (From Smith and Lin 1982.)

- A downward displacement, similar to that of the sinusoidal heating function, is produced near the region where the heating occurs. This relationship will be explained in Section 6.2.

- The upstream phase tilt of the thermally forced gravity waves is evident above the heating level. The vertical displacement at the heating level is repeated every 6.28 km ($2\pi / l$). The surface perturbation pressure is shown in the lower panel of Fig. 6.4. The hydrostatic equation indicates that the surface pressure is an integral measure of the temperature or density anomaly aloft. The thermodynamic equation implies that the heating directly causes the temperature anomaly, while thermally-induced vertical motion causes it indirectly.

- The relationship between the system's thermal response and the basic flow will be discussed in the following section as it is related to a transient flow over a heat source.

6.2 Transient flows over an isolated heat source

6.2.1 Flow responses to pulse heating

- The basic dynamics of flow responses to pulse heating can be studied by considering a two-dimensional, inviscid, nonrotating, hydrostatic, Boussinesq uniform flow over a heat source. The governing equation can be deduced from (3.2.1),

$$\left(\frac{\partial}{\partial t}+U\frac{\partial}{\partial x}\right)^2\frac{\partial^2 w'}{\partial z^2}+N^2\frac{\partial^2 w'}{\partial x^2}=\left(\frac{g}{c_pT_o}\right)\frac{\partial^2 q'}{\partial x^2}. \qquad (6.2.1)$$

The above equation is similar to (4.2.1). To solve (6.2.1), we again apply *Green's function method* in the vertical direction.

[Details of the solutions] Taking the Fourier transform in x and the Laplace transform in t of the above equation (which transforms $w'(t,x,z)$ into $\hat{w}(s,k,z)$; see Appendix 6.1), yields

$$\frac{\partial^2\hat{w}}{\partial z^2}+\lambda^2\hat{w}=\frac{g\lambda^{\ 2}}{c_pT_oN^2}\hat{q}, \qquad (6.2.2)$$

where $\lambda\equiv iNk/(s+iUk)$, and $\mathrm{Re}(s)>0$ is assumed. Assuming the heating is released in a short pulse at a single level, $z = 0$, in an unbounded fluid,

$$q'(t,x,z)=\left(\frac{Q_o b^2}{x^2+b^2}\right)\delta(z)\delta(t), \qquad (6.2.3)$$

taking the Fourier and Laplace transforms of the above heating function and substituting it into (6.2.2) gives

$$\frac{\partial^2 \hat{w}}{\partial z^2}+\lambda^2\hat{w}=\frac{gQ_o b\lambda^2 e^{-bk}\delta(z)}{c_p T_o N^2}. \qquad (6.2.4)$$

Similar to the steady state problem, the solution for the vertical displacement can be obtained by applying the appropriate upper, lower, and interface conditions, yielding

$$\hat{\eta}(s,k,z)=\left(\frac{gQ_o b}{2c_p T_o N}\right)\frac{ke^{-bk}e^{-Nk|z|/(s+iUk)}}{(s+iUk)^2}. \qquad (6.2.5)$$

In the above equation, the vertical displacement is related to the vertical velocity through $w'=D\eta/Dt=\partial\eta/\partial t+U\partial\eta/\partial x$. Taking the inverse Laplace transform in s (Appendix 6.1) and the inverse Fourier transform in k (Appendix 5.1) of the above equation, leads to (Lin and Smith 1986)

$$\eta(t,x,z)=\left(\frac{gQ_o bte^{-bK}}{2c_p T_o N}\right)\left\{(\mathrm{b}^2-X^2)\cos(KX)+2bX\sin(KX)\right\}, \qquad (6.2.6)$$

where $K=Nt|z|/(X^2+b^2)$ and $X=x-Ut$ is the horizontal coordinate in the reference frame moving with the basic wind. The flow response in a moving frame is analogous to a pulse heating in a quiescent fluid, as discussed in Section 6.1.

As in the steady state problem, the solution for heating that is distributed in a layer can be obtained through the superposition of the heating at a particular level within the heating layer, while the solution for a half-plane with a rigid lower surface can be obtained from that in an unbounded fluid, (6.2.6), by the *method of images* (e.g. Hildebrand 1976).

In the method of images, the solution is obtained by superimposing a solution to the original forcing and that of its mirror image at the same distance below the rigid boundary (z = 0 in this case). The solution for a heating layer can be obtained by integrating the solution of a single level across the heating layer.

The vertical displacement at the center of the heating layer ($z = z - d$ to $z + d$), where d is the half-depth of the heating layer, in the unbounded fluid can be derived to be

$$\tilde{\eta} = \left(\frac{1}{\tilde{x}^2 + 1}\right)\left\{1 - e^{-\tilde{t}/(\tilde{x}^2+1)}\left[\tilde{x}\sin\left(\frac{\tilde{x}\tilde{t}}{\tilde{x}^2+1}\right) + \cos\left(\frac{\tilde{x}\tilde{t}}{\tilde{x}^2+1}\right)\right]\right\}, \qquad (6.2.7)$$

where $\tilde{x} = (x - Ut)/b$, $\tilde{t} = Ndt/b$, and $\tilde{\eta} = (c_p T_o N^2 / gQ_o)\eta(t, x, z = 0)$. We are interested in the flow response to pulse heating in two regions: (a) the region of drifting heated air and (b) the region of the initial heating.

Figure 6.5a shows the evolution of the vertical displacement around the center of drifting disturbance.

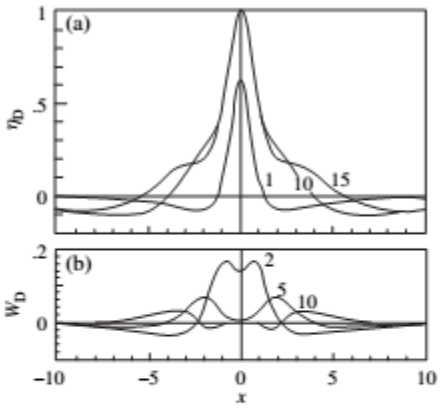

Fig. 6.5 (a) The vertical displacements at the heating level of the pulse heat source in a frame moving with the basic wind. The solution is given by (6.2.7). The three curves represent $\tilde{\eta}$ at $\tilde{t} = 1$, 10, and 15. Note that there is a strong updraft near the drifting center and two regions of compensated downdrafts to the sides of the growing updraft. (b) The normalized vertical velocities at $\tilde{t} = 2$, 5 and 10. The horizontal coordinate is nondimensionalized as in (6.2.7). (Adapted after Lin and Smith 1986.)

- This displacement occurs in a reference frame that is moving with the basic wind. The fluid's early response to the heating is an upward displacement at the drifting center and downward displacements at the upstream and downstream sides of the growing disturbance.

- The weak downward displacements are necessary because they compensate for the upward motion at the center. Mass continuity requires this downward displacement.

- The vertical displacement at the drifting center ($\tilde{x} = 0$) grows according to the function $\exp(1 - e^{-\tilde{t}})$. The final vertical displacement $\tilde{\eta}(t = \infty, x, z)$ is proportional at all points to the total amount of heat received by that air parcel. This displacement can be found by letting $\tilde{t} \to \infty$ in (6.2.7)

$$\tilde{\eta}_D(t = \infty, x, z) = \frac{1}{\tilde{x}^2 + 1}, \quad \text{for } z_o - d \le z \le z_o + d, \qquad (6.2.8)$$

which is proportional at all points to the total amount of heat received by the air parcel. Figure 6.5b shows the nondimensional vertical velocity at the center of the pulse heating, which corresponds to Fig. 6.5a.

- Once the updraft at the drifting center weakens, the fluid in the adjacent regions can rise. Subsequently, two updrafts develop and propagate outward.

- This action is analogous to the left and right moving waves in a two-dimensional shallow water system. These updrafts will overcome the downward displacement produced earlier and generate upward displacement at a later time, as can be seen

from Fig. 6.5a. When this time is reached, the original disturbance will have split in two.

- To find the flow response at the heating center, we set $x = 0$ in $\tilde{x}$ in (6.2.7). The nondimensional vertical displacement at the origin of the initial pulse heating can thus be obtained

$$\tilde{\eta}_o = \frac{1-\exp[-\tilde{t}/F_r(\tilde{t}^2+1)]}{\tilde{t}^2+1}\left\{\tilde{t}\sin\left(\frac{\tilde{t}^2}{F_r(\tilde{t}^2+1)}\right)+\cos\left(\frac{\tilde{t}^2}{F_r(\tilde{t}^2+1)}\right)\right\}, \quad (6.2.9)$$

where $F_r \equiv U/Nd$ is the *thermal Froude number*.

The above equation reduces to $\tilde{\eta}_o \approx (1/\tilde{t})\sin(1/F_r)$ when $\tilde{t} \to \infty$. Therefore, the response of the flow at the heating center ($x = 0$) is strongly dependent on F_r, and changes sign at $F_r = 1/n\pi$. The vertical displacement at the heating center decreases as $1/\tilde{t}$ when $\tilde{t} \to \infty$, as shown in Fig. 6.6.

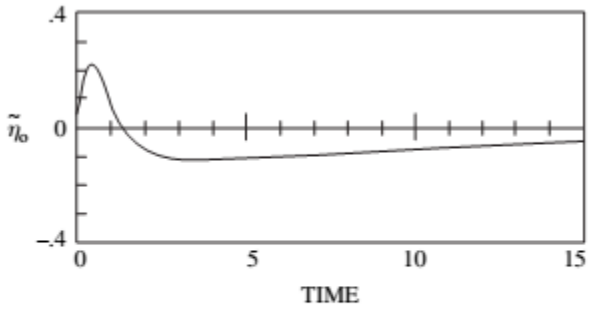

Fig. 6.6 The vertical displacement at the origin of the pulse heating. The solution is given by (6.2.9). Note that the response of $\tilde{\eta}_o$ is an upward displacement followed by a downward displacement, as the heated air drifts away. The time and vertical displacement are nondimensionalized. (From Lin and Smith 1986.)

- The response of the flow at the origin of the pulse heating is an upward displacement, followed by a downward displacement as the heated air drifts away.

- For a stronger basic flow (larger F_r), the downward displacement produced later in the process is associated with the compensating downdraft as the growing updraft drifts downstream due to the advection effect. On the other hand, for a weaker basic flow (smaller F_r), the advection effect is weaker and the growing updraft dominates the flow response near the heating center and produces an upward displacement. This *advection mechanism* helps explain the negative phase relationship between the vertical displacement and heating shown in Figs. 6.1 and 6.4.

6.2.2 Flow responses to steady heating

- As shown in Figs. 6.1 and 6.4, steady heating in a moving airstream produces a curiously negative relationship between heating and vertical displacement. That is, heating (cooling) produces a downward (upward) displacement in the vicinity of the heat source (sink). This effect is directly related to the steadiness of the heating and can be explained as follows:

Taking $b \to 0$ and keeping $Q_o b$ constant in (6.2.6)

gives the vertical displacement of a moving stratified airstream to a point heat source that is released initially as a pulse

$$\eta(t,x,z) = \frac{-Q_o bt}{2\pi N\tilde{x}^2}\cos\left(\frac{Nzt}{\tilde{x}}\right), \qquad (6.2.10)$$

where $\tilde{x} = (x - Ut)/b$. Since we are interested in the response near the origin of the heating, $(x,z) = (0,0)$, the above equation reduces to

$$\eta(t,0,0) = \frac{-Q_o b^3}{2\pi NU^2 t}. \qquad (6.2.11)$$

Thus, the air is displaced downward proportional to t^{-1} at the origin of a pulse heating, consistent with (6.2.9) as $\tilde{t} \to \infty$.

The steady state heat source may be regarded as a succession of very short heat pulses, which leads to an accumulated downward displacement by individual pulse heating events at the origin of heat source. This advection mechanism is consistent with the group velocity argument (Bretherton 1988). In the group velocity argument, the 1/*t* decay of the displacement is shown to be a geometrical consequence of dispersion in two dimensions. The growing response to a steady heating is understood as the result of energy being pumped into the gravity wave modes, whose group velocity is near zero, faster than it can spread in physical space due to dispersion.

In addition to the advection mechanism and group velocity argument, an alternative explanation of the negative relationship between vertical displacement and thermal forcing can be made using the energy budget. A linearized steady state energy equation may be derived through a method similar to that used in deriving (4.4.5). Thus, by excluding the basic shear terms and including the diabatic heating term, we obtain

$$\frac{\partial}{\partial x}(EU + p'u') + \frac{\partial}{\partial z}(p'w') = \left(\frac{\rho_o g^2}{c_p T_o N^2 \theta_o}\right)\theta' q', \qquad (6.2.12)$$

where $E = (\rho_o / 2)[u'^2 + (g\theta'/N\theta_o)^2]$ is the perturbation wave energy in a hydrostatic atmosphere. According to the above equation, the addition of thermal energy to the system requires that steady heating be added where the air is warm or the air density is low. This condition implies that the perturbation flow field must adjust itself so that the regions of negative density anomaly (negative displacement) may receive the heat.

The gravity waves produced by a pulse heating in an unsheared flow are symmetric about the heating center and impart no net momentum flux to the flow. Thus, no vertically propagating gravity waves are produced. However, a steady heating or cooling can generate vertically propagating gravity waves. The vertical displacement for the steady state heating can be obtained by integrating (6.2.6). Figure 6.7 shows an example in which a steady state heating is imposed $t = 0$ in an unbounded stratified fluid. The fluid has two separate responses. First, a region of upward displacement is initially generated at the origin of the heat source and is subsequently advected downstream by the basic wind. The amplitude of the displacements continues to grow with time. Note that the peak of the upward displacement appears to propagate downstream with a slower speed than the basic flow. Second, there is also a downward displacement in the vicinity of the stationary source, which develops at a much slower rate than that of the drifting disturbance.

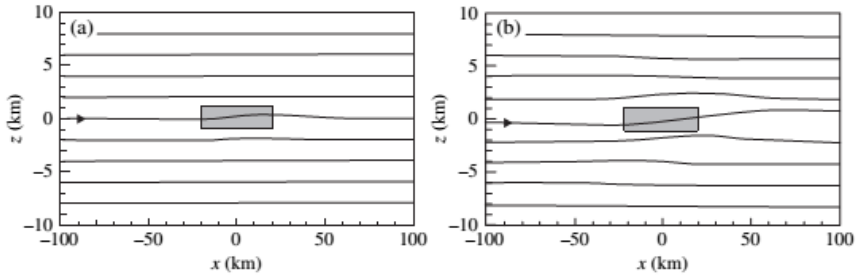

Fig. 6.7 Vertical displacement of an unbounded, hydrostatic atmosphere to a steady state heating (shaded) imposed at $t = 0$. Two times are shown: (a) 3000 s, and (b) 7000 s. The solution can be obtained by integrating (6.2.6) for a layer from $z = z_o - d$ to $z_o + d$ and in time. The flow parameters used are: $U = 10$ m s^{-1}, $N = 0.01$ s^{-1}, $T_o = 273$ K, $Q_o = 1$ J kg^{-1} s^{-1}, $b = 20$ km, $d = 1$ km, and $z_o = 0$ km. (From Lin and Smith 1986.)

6.3 Applications to mesoscale circulations

6.3.1 Density current formation and propagation

- Figure 6.8 shows the response of a two-dimensional, hydrostatic, stratified flow to a prescribed cooling, which represents a quasi-steady cooling due to rain evaporation, in the subsaturated layer beneath a thunderstorm, as simulated by a nonlinear numerical model.

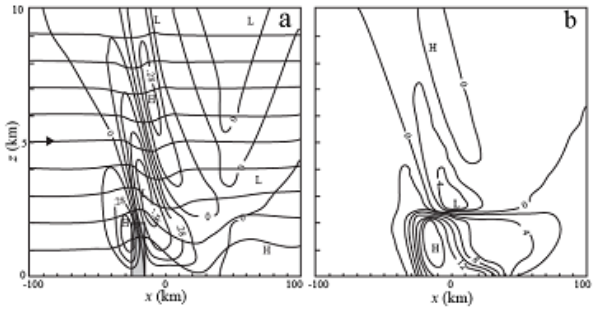

Fig. 6.8: Response of a two-dimensional, hydrostatic, stratified flow to a prescribed cooling, which represents a quasi-steady evaporative cooling of rainfall under a thunderstorm, as simulated by a nonlinear numerical model at 4000 s: (a) vertical displacement (horizontal curves) and vertical velocity (contours) and (b) perturbation density. The flow parameters used are: U = 15 ms^{-1} and N = 0.01 s^{-1}. The prescribed cooling is concentrated in the shaded region. (Adapted after Lin and Smith 1986)

- The upward vertical displacement in the vicinity of the heat sink resembles the flow structure near the front of a squall line, and may provide a possible mechanism for its maintenance. The negative phase relationship between the cooling and the vertical displacement (Fig. 6.8a) can be explained by the advection mechanism and group velocity argument discussed earlier. The vertical velocity field

indicates that flow convergence near the surface causes an upward motion upstream of the heat sink due to mass continuity, a motion that is responsible for the upward vertical displacement.

- Note that a hydrostatic gravity wave is generated above the heat sink. The density field shows that a pool of cold air exists near the stationary heat sink (Fig. 6.8b). The strong density gradient in front of the heat sink (x = -35 km) may be regarded as an upstream *gust front* produced by a density current. The high-density region is related to the *mesohigh*, often observed under the strong downdraft region. On the downstream side, the density gradient is weaker than on the upstream side due to the advection of the cold air.

- In fact, for a uniform, stably stratified flow with prescribed cooling, flow responses are controlled by two nondimensional parameters, $U/(Q_o L d)^{1/3}$ and $\pi U / Nd$, where U is the basic flow speed, $Q_o = (g/c_p T_o)q'$ is the cooling rate, and d and L are the depth and width of the cooling region, respectively (Raymond and Rotunno 1989).

- The second nondimensional number ($\pi U / Nd$) is directly proportional to the thermal Froude number ($F_r = U / Nd$) defined in (6.2.9). Based on these two nondimensional numbers, four flow regimes are then identified: (a) supercritical relative to both gravity waves and cold air outflow, (b) subcritical

relative to gravity waves and supercritical relative to cold air outflow, (c) subcritical to both gravity waves and cold air outflow, and (d) supercritical relative to gravity waves and subcritical relative to cold air outflow.

- If the flow is subcritical relative to the gravity waves, then the gravity waves can propagate upstream against the basic flow.

- Similarly, if the flow is subcritical relative to cold air outflow, then a density current can form and propagate upstream against the basic flow.

- These four flow regimes are shown in Fig. 6.9.

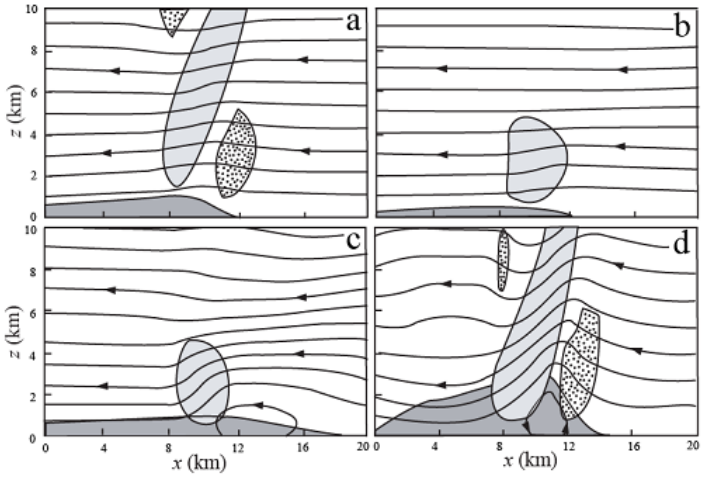

Fig. 6.9: Based on $F = U/(Q_o L d)^{1/3}$ and $G = \pi U / N d$, four flow regimes are identified: (a) supercritical relative to both gravity waves and cold air outflow (both F and G are large), (b) subcritical relative to gravity waves and supercritical relative to cold air outflow (F small, G large), (c) subcritical to both waves and cold air outflow (both F and G are small), and (d) supercritical relative to gravity waves and subcritical relative to cold air outflow (F large, G small). Streamlines are denoted by solid lines, while regions of significant vertical motion are shaded. Dotted (light shaded) area indicates upward (downward) motion. Cold pools are denoted by dark shading. (Adapted after Raymond and Rotunno 1989)

- This study is extended (Lin et al. 1993) to investigate the flow response and the interaction between gravity waves and cold air outflows. It is found that a density current is able to form or is destroyed depending on the interaction between the traveling gravity wave and the cold air outflow.

6.3.2 Heat island circulations

A *heat island* is defined as a local area which is significantly warmer than its surroundings. When this happens in a metropolitan area, it is referred to as an *urban heat island*.

- The linear theory discussed in the previous section has been extended to the case of weakly nonlinear flow (Chun and Baik 1994; Baik and Chun 1997).

- The nonlinear component of the solution indicates that the downward or upward motion downstream depends on the heating depth, or the thermal Froude number (F_r).

  When F_r is small (Fig. 6.10) but still within a valid range for the perturbation expansion to be valid, the linear and weakly nonlinear effects work together constructively to produce enhanced upward motion on the downstream side of the heat island. This motion occurs not far from the heating center.

- These findings might explain to a greater extent the precipitation enhancement observed downstream of a heat island than linear effects alone (Hjelmfelt 1982). The effect of rainfall enhancement is often explained by the addition of condensation nuclei introduced by the urban heat island into the airstream.

- However, from the above theories, the urban heat island effect can create a stationary heating source that produces ascent under a certain range of the thermal Froude numbers. Thus, a combined study of the addition of condensation nuclei and of thermal effects may be required to fully understand this phenomenon.

6.3.3 Moist convection

- Application of the linear theory involving prescribed cooling is useful for studying the dynamics of snow melting-induced mesoscale circulations. Although the latent heat of melting is eight times smaller than the latent heat of evaporation, melting is concentrated in a shallow layer of near 0^{o}C temperature. Thus, the cooling rate induced by melting can be comparable to that induced by evaporation (Robichaud and Lin 1989).

- Most rainfall in the midlatitudes is initiated through ice formation processes followed by melting. The transition from the solid to liquid phase normally takes place in an atmospheric layer that appears as a layer of enhanced reflectivity called a *bright band*.

- Theoretical studies of flow responses of a stratified flow to a prescribed temperature perturbation were found to be useful for understanding the dynamics of snow melting-induced mesoscale circulations (e.g., Szeto et al. 1988; Lin and Stewart 1991). It is found that thermally induced circulations have a length scale similar to that of the temperature perturbations that produce them. The updraft branch of the thermally induced circulation may enhance precipitation in a saturated environment.

- The transient flow responses to prescribed heating and cooling obtained from linear theories can also help us understand the mean flow and shear effects in the adjustment to latent heating in cumulus cloud fields and, consequently, to improve the schemes of cumulus parameterization (Bretherton 1993).

6.3.4 Gravity wave generation and propagation

- Section 4.2 introduced examples of theoretical studies of stratified flow over prescribed heating or cooling to gravity wave generation. These types of studies can also be applied to wave propagation.

- For example, based on analytical solutions of the transient linear response of a quiescent, two-dimensional, nonrotating atmosphere to prescribed low-level steady heating, it is found that two modes exist in the flow when the atmosphere is bounded above by a rigid top: (1) a deep fast-moving mode, responsible for subsidence warming throughout the depth of troposphere, and (2) a slower

moving mode, corresponding to midlevel inflow and lower- and upper-level outflows (Fig. 6.11a; Nicholls et al. 1991).

- The linear hydrostatic solution shows a region of upward motion extending in a jetlike flow from the top of the heat source (2.5 km). Upward propagating gravity waves are clearly shown by the vertically tilted phase lines. Regions of compensating weak downward motion are thus produced and propagated outward from the heating center.

- Note that the positive phase relationship between the vertical motion and diabatic heating is anticipated for a low thermal Froude number flow, which is 0 in this extreme case because $U = 0$. The nonlinear, numerically simulated flow response for an atmosphere with constant stratification is similar to the response obtained through linear theory (Fig. 6.11b).

- The numerical simulation is more realistic: the atmosphere is stable in the lower troposphere, less stable in the upper troposphere and more stable in the stratosphere. Significant wave reflection occurs under these conditions.

- For a rigid-lid solution, the outward-propagating downward motion occurs at $x = \pm 160$ km corresponding to the $n = 1$ mode, while vertically oriented gravity waves with shorter vertical wavelengths occur at $x = \pm 60$ km below 5 km corresponding to the $n = 2$ mode. These propagating waves are similar in structure to the gravity waves produced in two-dimensional numerical simulations of convection occurring over the Florida peninsula.

- Another example of gravity wave generation and propagation studied by prescribing diabatic cooling is shown in Fig. 4.3, in which a nonhydrostatic model is used to simulate a density current in an environment characterized by a complex stratification and vertical wind. It is found that the density current generated gravity waves, which then propagated along the current itself. Figure 4.4 provides an additional example of gravity waves generated in the stratosphere by moist convection.

6.4 Effects of shear, three dimensionality and rotation

6.4.1 Two-dimensional shear flows

The effects of vertical shear on thermally forced flow, such as squall lines and convective cloud bands, are well documented. One example is the moist convection associated with midlatitude squall lines, such as shown in Fig. 6.12. In particular, this squall line exhibits a critical level near 6 km. Note that the critical level coincides with the wind reversal level in a steady-state flow because the phase speed is 0 (Sec. 3.8; Sec. 5.3). In this section, we will investigate the effects of vertical shear in a thermally forced flow in a simple environment. This will help us understand its effects in more complicated mesoscale circulations.

The effects of shear flows with thermal forcing can be discerned by considering a two-dimensional, unbounded, steady-state, small-amplitude, non-rotating, inviscid, Boussinesq, shear flow with constant buoyancy frequency over a heat source,

$$U^2 \frac{\partial^2}{\partial x^2}\left(\frac{\partial^2 w'}{\partial x^2}+\frac{\partial^2 w'}{\partial z^2}\right)-UU_{zz}\frac{\partial^2 w'}{\partial x^2}+N^2\frac{\partial^2 w'}{\partial x^2}=\left(\frac{g}{c_pT_o}\right)\frac{\partial^2 q'}{\partial x^2}. \qquad (6.4.1)$$

The above equation is a special form of the *Taylor-Goldstein equation*, (3.7.19) except that $\partial/\partial t = 0$ and with the addition of the diabatic heating term. To simplify the problem, we further assume the basic wind varies linearly with height,

$$U(z) = \alpha z, \qquad (6.4.2)$$

where $\alpha = \partial U/\partial z$ and $z = 0$ is the critical (wind reversal) level. The mathematics can be further simplified by assuming that the heating function is separable in *x* and *z* directions,

$$q'(x,z) = Q_o f(x) g(z). \qquad (6.4.3)$$

and the flow is hydrostatic ($\partial^2/\partial x^2 << \partial^2/\partial z^2$). Substituting (6.4.2) and (6.4.3) into (6.4.1) and taking the Fourier transform in x yields

$$\frac{\partial^2 \hat{w}}{\partial z^2}+\left(\frac{N}{\alpha z}\right)^2 \hat{w} = \left(\frac{gQ_o}{c_pT_o\alpha^2 z^2}\right)\hat{f}(k)g(z). \qquad (6.4.4)$$

Once the heating function is known, the above problem can be solved in a way similar to that used to solve the uniform flow problem discussed in Sections 3.8 and 6.1. For example, if we take a prescribed isolated heating contained in the layer from the surface to a level below the critical level H_1, $q'(x) = Q_o f(x)$ for $|z| \le H_1$, the general solution of (6.4.4) is

$$\hat{w}(k,z) = Az^{1/2+i\mu}, \quad z < -H_1 \qquad (6.4.5a)$$

$$\hat{w}(k,z) = Bz^{1/2+i\mu} + Cz^{1/2-i\mu} + \left(\frac{gQ_o}{c_pT_oN^2}\right)\hat{f}(k), \quad |z| \le H_1 \qquad (6.4.5b)$$

$$\hat{w}(k,z) = Dz^{1/2-i\mu}, \quad H_1 < z, \qquad (6.4.5c)$$

where $\mu^2 = Ri - 1/4$ and $Ri\,(= N^2/\alpha^2)$ is the *Richardson number*. Similar to the boundary conditions discussed in Section 3.8, the upper radiation condition has been imposed in the lower and upper layer. Following a similar procedure as in Section 6.1, the interface conditions at $z = -H_1$ can be derived. They require both $\hat{w}$ and $\hat{w}_z$ to be continuous across the interface. Special attention should be paid to the solution at the critical level, which is similar to that discussed in Section 3.8. Figure 6.13 shows the streamlines and vertical velocity field for a two-dimensional, steady-state, unbounded, stratified, shear flow with a critical level over an isolated heat source, similar to that in Fig. 3.14b except that the atmosphere is unbounded and there is heating at the critical level. The Richardson number of the basic flow is $Ri = 1$. The presence of thermal forcing in the vicinity of the critical level significantly modifies the flow. Below the critical level, the fluid particle undergoes a downward motion upstream (on the left side) of the heating center, followed by an ascending motion downstream (Fig. 6.13a). This broad descending motion can be explained by the advection effect and group velocity argument discussed in Section 6.2. In the vicinity of the critical level, however, the fluid particle in the lower layer experiences a strong upward motion near the heating center, crosses the critical level, and then returns to the left of the domain in the upper layer. The flow near the concentrated heating region is strongly dominated by an upward motion (Fig. 6.13b). The in-phase relationship between the vertical motion and the heating, which is to be explained in the next paragraph, is important in order to maintain the convection. Away from the concentrated heating region, the upstream phase tilt induces upward (downward) propagation of wave energy in the upper (lower) layer. When applied to the dynamics of moist convection, the condensational heating in the vicinity of the critical level appears to facilitate the flow interaction above and below the critical level. In fact, the flow circulation in the vicinity of the heating area is somewhat similar to that associated with the squall line observed on 22 May 1976 (Fig. 6.12).

The in-phase relationship between the vertical motion and the heating in the heating region at the critical level can be explained by considering the steady-state thermodynamic equation,

$$U\frac{\partial \theta'}{\partial x} + \frac{N^2\theta_o}{g}w' = \frac{\theta_o}{c_p T_o}q'. \qquad (6.4.6)$$

At the critical level ($z = 0$), w' is proportional to q' because the basic wind disappears. This also means that no temperature anomalies are produced directly by the heating at the critical level. In fact, at the critical level, the nondimensional form of the relationship between vertical velocity and diabatic heating may be expressed as $\tilde{w} = \tilde{q}/Ri$. Thus, the vertical velocity at the critical level increases as *Ri* decreases for a constant heating rate. As discussed in Section 3.8, for $0.25 < Ri < 2.0$, a significant amount of the wave energy is reflected and some of it is also transmitted through the critical level. This also helps to explain the strong interaction between the flow above and below the critical level for cases where $Ri = 1$ (Figs. 3.14b and 6.13). For $Ri < 0.25$, *overreflection* can occur.

Note that a small perturbation in the horizontal velocity field may easily exceed the basic horizontal flow velocity in the vicinity of the critical level, thereby resulting in a highly nonlinear flow. In order to study the nonlinear effects, a nonlinear numerical simulation is conducted with a setting similar to that in Fig. 6.13. Figure 6.14a shows the nonlinear response in a thermally forced flow. The basic wind has a hyperbolic tangent profile with *Ri* = 0.1 at the wind reversal level ($z_i = 5$ km). The nonlinear transient response (Fig. 6.14a) is approximately similar to the steady state linear solution for a linear shear flow over isolated heating (Fig. 6.13) and the transient linear flow response (Fig. 6.14b). The closed circulation centered at the critical level resembles the squall line observation shown in Fig. 6.12 and simulated by the wave-CISK model (Fig. 4.19b). The major difference of the nonlinear response relative to the linear response is that the former is stronger and more compact. The following energy argument can be used to explain the *upshear phase tilt* of the upward motion in the shear layer, as shown in Fig. 6.14. Since there is shear instability, the local rate of change in total perturbation energy is positive, which, in turn, requires the vertical momentum flux term (integral of $-\rho_o U_z \overline{uw}$) to be negative in the whole domain for $U_z > 0$. This condition requires an upshear tilt of the vertical motion. This aspect will be further discussed in Section 7.1.

This type of approach for treating thermally forced flow in simple environments has been taken to help understand various mesoscale circulation problems in the atmosphere. Related developments include: (a) squall line initialization in numerical models (Crook and Moncrieff 1988), (b) the response of a nonlinear shear flow with a critical level to a steady cooling (Lin and Chun 1991), (c) amplification mechanisms for melting-induced circulations (Robichaud and Lin 1989), (d) the effects of evaporative cooling in a three-layer flow with a critical level (e.g. Chun and Lin 1995), (e) the role of internal gravity waves in modifying the behavior and structure of a simulated squall line (Schmidt and Cotton 1990), and the effects of variable wind shear on the mesoscale circulations (Reuter and Jacobsen 1993), (f) the transient responses in a shear flow with critical level (Baik et al. 1999), and (g) the convective gravity wave drag parameterization (Song and Chun 2005).

6.4.2 Three-dimensional nonrotating flows

The small-amplitude equation governing the vertical velocity for a steady state, three-dimensional, stratified, incompressible, Boussinesq, non-rotating flow can be reduced from (2.2.14)-(2.2.18) to the following,

$$\left(U\frac{\partial}{\partial x}+V\frac{\partial}{\partial y}+\nu\right)^2\nabla^2 w'-\left(U\frac{\partial}{\partial x}+V\frac{\partial}{\partial y}+\nu\right)\left(U_{zz}\frac{\partial}{\partial x}+V_{zz}\frac{\partial}{\partial y}\right)w'\frac{\partial^2 w'}{\partial x^2}$$

$$+N^2\nabla_H^2 w'=\left(\frac{g}{c_p T_o}\right)\nabla_H^2 q'. \qquad (6.4.7)$$

The procedure involved in obtaining the analytical solution is also similar to that in the mountain wave theory described in Section 5.4.1 except that the Green's function method is employed here to solve the problem with interface boundary conditions.

By considering a special case with uniform wind $U(z) = U$ and $V = 0$, and a bell-shaped heat source with circular contours,

$$q'(x, y, z) = \frac{Q_o \delta(z)}{(x^2/b^2 + y^2/b^2 + 1)^{3/2}}, \tag{6.4.8}$$

in an unbounded atmosphere, the problem can be solved analytically in the Fourier space and then transformed back to the physical space by applying a fast Fourier transform (FFT) algorithm.

Figure 6.15 shows the nondimensional vertical displacement of a three-dimensional, hydrostatic, continuously stratified, uniform flow over an isolated shallow heat source added at $\tilde{z} = 0$. The surface, assumed to be flat, is located at $\tilde{z} = -\pi$. The basic flow is directed from left to right. The fluid response to the heating at the heating level ($\tilde{z} = 0$) is a downward displacement upstream of the prescribed heat source followed by an upward displacement downstream (Fig. 6.15b). This response is similar to that given by the thermally-induced two-dimensional flow with high Froude number discussed earlier in this chapter. The region of disturbance generally widens as one moves above and below the heating level. At $\tilde{z} = \pi/2$, a V-shaped pattern, which is similar to the U-shaped disturbance as discussed in Chapter 5, in the region of upward displacement forms above the heating center (Fig. 6.15c). This region of upward displacement shifts upstream as one moves higher as required by the upper radiation condition. This upstream movement allows the heating-generated energy to propagate upward to infinity. At $Nz/U = \pi$ (Fig. 6.15d), the V-shaped region of upward displacement shifts further upstream and widens in the cross-wind direction. In addition, a region of downward displacement also forms downstream of the V-shaped region of upward displacement. The response is almost periodic in the vertical and the flow fields at $Nz/U = -\pi/2$ and $\pi/2$ (Figs. 6.15a and 6.15c) are quite similar.

The flow behavior is similar to the three-dimensional flow over an isolated mountain and the formation of a V-shaped pattern of upward displacement can be explained using a group velocity argument (Fig. 5.17; Smith 1980). The pattern is produced by basic wind advection of the heating-generated upward propagating gravity waves, while the wave energy is concentrated in the V-shaped region trailing downstream. The hydrostatic group velocities (5.4.23) can be extended for a nonhydrostatic flow,

$$c_{gx} = U\left(\frac{l^2 + k^4U^2/N^2}{k^2 + l^2}\right), \tag{6.4.9a}$$

$$c_{gy} = -U\left(\frac{kl(1 - k^2U^2/N^2}{k^2 + l^2}\right), \tag{6.4.9b}$$

$$c_{gz} = \frac{U^2k^2(1 - k^2U^2/N^2)^{1/2}}{N(k^2 + l^2)^{1/2}}. \tag{6.4.9c}$$

The propagation of the wave energy associated with quasi-steady waves forced by a prescribed heating in an unbounded, nonhydrostatic, shear flow is sketched in Fig. 6.16. Above the heating, the energy propagates upward and upstream relative to the air (c_{ga+}), but is then advected downstream by the basic flow. Thus, the wave energy is along the direction of c_{gh+} or c_{gh-} relative to the heat source. The nonhydrostatic effects are the main cause of the formation of the disturbance's repeating, damped oscillations. The wave energy is concentrated in the region enclosed by the parabola:

$$y^2 = \left(\frac{Nz}{U}\right)\left\{\frac{[1-(kU/N)^2]^{3/2}}{(k^2+l^2)^{1/2}(1+k^4U^2/N^2l^2)}\right\}x. \qquad (6.4.10)$$

The response to a heating layer from z_1 to z_2 can be obtained by taking a continuous superposition (i.e. integration) of $w'(x,y,z_o)$ with respect to z_o, where $z_1 \le z_o \le z_2$, and $w'(x,y,z_o)$ is the Green's function solution for heating applied at a single level z_o. In the absence of a basic wind (U = 0), the vertical velocity distribution corresponds to the axisymmetric shape of the heat source, thus resulting in upward motion over the region of heating. This in-phase relation of the vertical displacement and heating is present over a wide range of values of the basic wind in the three-dimensional flow. In contrast to the two-dimensional thermally-induced flow responses discussed earlier, only in strong basic winds does downward motion develop over the heating layer. Physically, this occurs because part of the flow is able to circumvent the isolated three-dimensional heat source. In a region where no thermal forcing exists, such as in Figs. 6.15a, c, and d, the temperature perturbation is inversely proportional to the vertical displacement according to $\theta' = -(N^2\theta_o/g)\eta$. In other words, the V-shaped regions of upward (downward) displacement will adiabatically produce cold (warm) air.

The above theory and its extension through the inclusion of vertical wind shear have been applied to explain the formation of the V-shaped cloud anvil over a thunderstorm cloud top, as observed via satellite imagery (e.g., Adler and Mack 1986). V-shaped cloud anvils have often been observed over severe midwestern thunderstorm cloud tops that rise above the tropopause level. These thunderstorm cloud tops normally are measured on a scale on the order of 10 km and are typically embedded in more diffuse V-shaped anvils with lateral widths of over 100 km and lengths of several hundred kilometers. Figure 6.17a shows the V-shaped cloud top features based on the analysis of a satellite image. Prominent features of this thunderstorm top are: (a) a region of lowest cloud top temperatures associated with the updraft air overshooting the tropopause, (b) a V-shaped region of lower equivalent blackbody temperature with the point of the V either at or above the cloud top, and (c) a region of higher temperatures 20-40 km downwind of the cloud top (i.e. the closed-in warm area), forming a cold-warm thermal couplet with (a). Figure 6.17b shows the vertical velocity field at z = 14 km predicted by a linear theory of hydrostatic flow over a prescribed heating distributed from z = 1.5 km to 12 km and a linear unidirectional vertical shear of the basic wind. The V-shaped region of upward (downward) displacement corresponds to the cold (warm) region resulting from adiabatic cooling (warming), which mimics the observed V-shaped cloud anvils over severe thunderstorms (e.g. Fig. 6.17a). The asymmetric, skewed V-

shaped cloud anvils result from the advection effects of directional shear flow. In addition to the thermal forcing, other mechanisms, such as the mechanical forcing by the cloud top (e.g., Heymsfield and Blackmer 1988), the mixing of stratospheric and cloud air (e.g., Adler and Mack 1986), and injection of the plume of cloud water vapor into the stratosphere (e.g., Wang 2003), have been proposed.

6.4.3 Three-dimensional rotating flows

Equations (5.1.1) – (5.1.4) can be extended to investigate the three-dimensional, steady-state, small-amplitude response of an inviscid, stratified, hydrostatic, Boussinesq flow on an *f* plane to a thermal forcing,

$$R_o u_{\tilde{x}} - v + \pi_{\tilde{x}} = 0, \tag{6.4.11}$$

$$R_o v_{\tilde{x}} + u + \pi_{\tilde{y}} = 0, \tag{6.4.12}$$

$$\pi_{\tilde{z}} - b = 0, \tag{6.4.13}$$

$$u_{\tilde{x}} + v_{\tilde{y}} + R_o w_{\tilde{z}} = 0, \tag{6.4.14}$$

$$b_{\tilde{x}} + w = \dot{q}, \tag{6.4.15}$$

where $R_o=U/fa$ is the *Rossby number*, π' ($=p'/\rho_o$) the *perturbation kinetic pressure*, b' ($=g\theta'/\theta_o$) the *perturbation buoyancy* and a the half-width (horizontal scale) of the heat source or sink. The nondimensional variables are defined as

$$(\tilde{x},\tilde{y}) = (x/a, y/a); \qquad \tilde{z} = z/H;$$

$$(u,v) = (u'/U, v'/U); \qquad w = w'b/R_o UH;$$

$$\pi = \pi'/(fUa) = p'/(\rho_o fUa); \qquad b = b'H/(fUa) = g\theta' H/(\theta_o fUa);$$

$$\dot{q} = q' gH/(c_p T_o U^2 f). \tag{6.4.16}$$

where $H=fa/N$ is the *deformation depth*.

Equations (6.4.11) – (6.4.15) can be combined into a single equation of w (with primes ignored)

$$R_o^{\,2}\frac{\partial^4 w}{\partial z^2 \partial x^2} + \frac{\partial^2 w}{\partial z^2} + \nabla_H^2 w = \nabla_H^2 \dot{q}. \tag{6.4.17}$$

Again, the mathematical problem can be solved using the Green's function method. For simplicity, we prescribe the surface heating as

$$\dot{q}(x,y,z) = h(x,y)e^{-z/\gamma}, \tag{6.4.18}$$

where γ is the nondimensional heating depth. Taking the double Fourier transform (Appendix 5.1) of the above equation in both x and y directions leads to

$$\frac{\partial^2 \hat{w}}{\partial z^2} + \left(\frac{K^2}{R_o^{\,2}k^2 - 1}\right)\hat{w} = \frac{K^2 \hat{h} e^{-z/\gamma}}{R_o^{\,2}k^2 - 1}. \tag{6.4.19}$$

The general solution of the above equation is

$$\hat{w} = Ae^{iKz/(R_o^2k^2-1)^{1/2}} + Be^{-iKz/(R_o^2k^2-1)^{1/2}} + \left(\frac{\gamma^2K^2}{(R_o^2k^2-1)+\gamma^2K^2}\right)\hat{h}e^{-z/\gamma}. \quad (6.4.20)$$

There exist two flow regimes for (6.4.20): (a) $R_o^2k^2 > 1$ and (b) $R_o^2k^2 < 1$.

For $R_o^2k^2 > 1$, the upper radiation boundary condition requires $B = 0$ in order to allow the energy to radiate upward. Over a flat surface, the lower boundary condition requires $w = 0$ at $z = 0$. Applying the lower boundary condition, the solution may be written as

$$\hat{w} = \left(\frac{-\gamma^2K^2\hat{h}}{(R_o^2k^2-1)+\gamma^2K^2}\right)\left[e^{iKz/(R_o^2k^2-1)^{1/2}} - e^{-z/\gamma}\right] \text{ for } R_o^2k^2 > 1. \quad (6.4.21)$$

For $R_o^2k^2 < 1$, the upper boundary condition requires the solution to decrease with height. Thus it requires $A = 0$ and the solution becomes

$$\hat{w} = \left(\frac{\gamma^2K^2\hat{h}}{(1-R_o^2k^2)-\gamma^2K^2}\right)\left[e^{-Kz/(1-R_o^2k^2)^{1/2}} - e^{-z/\gamma}\right] \text{ for } R_o^2k^2 < 1. \quad (6.4.22)$$

As long as the heating function, $h(x,y)\exp(-z/\gamma)$, is known, the solutions in the physical space can be obtained by performing inverse double Fourier transforms on (6.4.21) and (6.4.22). Because the inverse Fourier transform tends to be analytically intractable, a numerical method, such as a FFT subroutine, is often employed.

Consider a bell-shaped warm region as

$$\Theta'(x,y) = \frac{\Theta_o}{(x^2/a^2 + y^2/a^2 + 1)^{3/2}}, \quad (6.4.23)$$

where Θ_o is the maximum temperature anomaly of the warm region. To a first approximation, the diabatic heating rate associated with this specified warm region in a basic flow can be prescribed by $q'(x,y,0) = h'(x,y) \approx (c_pT_o/\theta_o)U\partial\Theta'/\partial x$ if the diabatic heating is mainly created and maintained by the horizontal temperature advection. Thus, a prescribed warm region, as described by (6.4.23), implies that a coupled diabatic heating and cooling are present in the basic flow. A more realistic representation of the sensible heating in the boundary layer could be used in a parameterization (see Chapter 14), but this would require a numerical model to solve the problem.

Figure 6.18a shows the response of an inviscid, hydrostatic, westerly flow to an isolated warm region near the surface. A region of upward motion concentrated in the warm region followed by a region of downward motion downstream is produced. Note that the descent that occurs upstream and over the heating region, as found in the two-dimensional case for a large R_o flow, is absent for most values of R_o in a three-dimensional flow due to lateral deflection. In addition, a cyclonic flow exists on the lee side of the warm region. The relatively strong advection effect moves the thermally forced cyclonic flow out of phase with the warm region. Note that the positive vorticity or cyclonic flow is not in phase with the low pressure for such a relatively high Rossby number flow. This occurs because the vertical motion still plays a significant role in the vorticity equation, $\hat{\zeta} = -K^2\hat{\pi} - iR_o^2k\hat{w}_z$. The vertical velocity field on the vertical plane across the heating center

has a strong upstream phase tilt, indicating that the wave energy produced by the diabatic heating and cooling associated with the prescribed warm region is able to propagate upward (Fig. 6.18b).

Figure 6.19 shows a case simimiar to that of Fig. 6.18 but with $R_o = 0.2$, which falls mostly in the regime $R_o^2 k^2 < 1$. A region of upward motion is produced on the heat source and followed by a downward motion to the downstream side of the heat source. These regions are a direct consequence of the heating and cooling that the prescribed heating function produces (Fig. 6.19a). The positive vorticity or cyclonic flow is more in phase with the warm region ($\theta' > 0$), and the low pressure, than in Fig. 6.18a. The flow response is similar to that predicted by the quasi-geostrophic theory except that the advection effect makes the disturbance stronger and allows a small amount of energy to propagate upward, as shown in Fig. 6.19b. The oscillating pattern on the lee side of the heat source (Fig. 6.19a) is caused by the dispersion associated with the evanescent inertia-gravity waves near the surface (Fig. 6.19b). For $R_o k << 1$, the first term inside the square bracket on the right hand side of (6.4.22) exponentially decays with height, therefore reducing the above fluid flow system to the *quasi-geostrophic flow* (Table 3.2). This is consistent with the results shown in Figs. 6.18 and 6.19.

The above three-dimensional theory has been extended to investigate various mesoscale problems with surface sensible heating associated with the Gulf Stream to the east of the Carolina coast, such as (a) lake effects on snowstorms in the vicinity of Lake Michigan (e.g. Hsu 1987; Sousounis and Shirer 1992), (b) coastal cyclogeneis in a baroclinic flow using a semi-geostrophic model (Lin 1990), and (c) coastal frontogenesis using a linear theoy (Riordan and Lin 1992) and a nonlinear primitive equation model (Xie and Lin 1996). For example, Fig. 6.20 shows a conceptual model under various basic wind conditions for the coastal frontogenesis associated with confluence zones and low-level jets. The coastal front forms at the confluence zone which is located at different points relative to the Gulf Stream front (i.e., the major axis of the heat source). Advection and rotational effects play a significant role in this thermally forced flow. This approach helps understand the basic dynamics of coastal frontogenesis as revealed in observational analyses (e.g. Riordan 1990), and sophisticated numerical simulations (e.g. Doyle and Warner 1993).

6.5 Dynamics of sea and land breezes

Sea and land breezes are the atmosphere's response to the differential surface heating across coastlines or shores of large lakes. They have been recognized among fishermen for several centuries and have been studied extensively by meteorologists for several decades to the present day. Figure 6.21 shows an example of a sea (lake)-breeze circulation observed near Chicago. Aside from the difference in forcing and circulation scales, the basic dynamics of sea-breeze circulations and lake-breeze circulations are identical. During the day, a smaller heat capacity causes the land to heat up more rapidly than the adjacent water surface. As a result, the air above the land surface expands and rises. At a height of about 1 km or the top of the convective boundary layer, the rising air spreads outward, creating an area of low pressure near the surface of the land. Less heating takes place over the adjacent water, thus causing the air pressure to be greater over water than over land. A *sea breeze* then develops as cooler air over the sea or lake is pushed

toward the land by the pressure gradient force. As a sea breeze advances toward land, a distinct boundary forms between cooler maritime air and the continental warmer air it displaces. This boundary is called the *sea breeze front*, and is characterized by often producing an abrupt drop in temperature by as much as 5 to 10°C as it passes overhead. The cooling effect of the sea breezes may reach a maximum distance of 100 km inland in the tropics and 50 km in midlatitudes. Across lakeshores, the scale of sea breezes is smaller. At night, the situation reverses: the land cools more rapidly than the sea and a *land breeze* develops.

The intensity and reach of sea and land breezes depends on location and time of year. For example, sea breezes are more frequent and intense in the tropics due to intense solar heating throughout the year. In the midlatitudes, sea breezes are more frequent during the warmer season, but the land breezes are often missing because the land does not always cool below the ocean temperature. In higher latitudes, the atmospheric circulations are often dominated by high- and low-pressure systems, making sea and land breezes less noticeable. Sea breeze circulations can be described in terms of the depth between the lower current and the upper "return" current, and their horizontal extent. Sea breeze depth ranges from just over 100 m to 1 km or higher. Dynamically, sea and land breezes are influenced by the diurnal variation of differential heating across the coastline, diffusion of heat, stability, the Coriolis parameter, and friction. Ideally, these effects can be understood and predicted by theoretical and numerical models. In the following, we will make a brief description of their fundamental dynamics.

6.5.1 Linear theories

The basic dynamics of sea and land breezes can be understood by considering the following set of equations governing the two-dimensional (across the coastline), small-amplitude, Boussinesq fluid flow,

$$\frac{\partial u'}{\partial t} + U\frac{\partial u'}{\partial x} - fv' = -\frac{1}{\rho_o}\frac{\partial p'}{\partial x} + F_{r1}, \tag{6.5.1}$$

$$\frac{\partial v'}{\partial t} + U\frac{\partial v'}{\partial x} + fu' = F_{r2}, \tag{6.5.2}$$

$$\frac{\partial w'}{\partial t} + U\frac{\partial w'}{\partial x} = -\frac{1}{\rho_o}\frac{\partial p'}{\partial z} + g\frac{\theta'}{\theta_o} + F_{r3}, \tag{6.5.3}$$

$$\frac{\partial u'}{\partial x} + \frac{\partial w'}{\partial z} = 0, \tag{6.5.4}$$

$$\frac{\partial \theta'}{\partial t} + U\frac{\partial \theta'}{\partial x} + \frac{N^2\theta_o}{g}w' = \frac{\theta_o}{c_p T_o}q', \tag{6.5.5}$$

where the F_{r1}, F_{r2}, and F_{r3} terms represent the viscous forces in the *x*, *y*, and *z*, directions, respectively. The above equation set is similar to (6.1.1) – (6.1.4) except that they are time-dependent, and contain viscosity and Coriolis force terms, as well as the *y*-momentum equation. A simple and common approach used to represent the viscous force in the planetary boundary

layer is to assume the *Fickian diffusion*, $(F_{r1}, F_{r2}, F_{r3}) = \nu\nabla^2(u', v', w')$, or $(F_{r1}, F_{r2}, F_{r3}) = \nu(\partial^2/\partial z^2)(u', v', w')$, where $\nabla^2 = \partial^2/\partial x^2 + \partial^2/\partial z^2$ and ν is the *eddy viscosity*.

Combining (6.5.1) – (6.5.5) with the frictional terms neglected and the thermal forcing term, regarded as a known function, leads to a single governing equation for *w'*

$$\left(\left(\frac{\partial}{\partial t}+U\frac{\partial}{\partial x}\right)^2+N^2\right)\frac{\partial^2 w'}{\partial x^2}+\left(\left(\frac{\partial}{\partial t}+U\frac{\partial}{\partial x}\right)^2+f^2\right)\frac{\partial^2 w'}{\partial z^2}=\frac{\partial^2 \dot{Q}}{\partial x^2}, \qquad (6.5.6)$$

where $\dot{Q} = (g/c_p T_o)q'$. Equation (6.5.6) reduces to (6.2.1) for a nonrotating and hydrostatic flow. Assuming

$$(w', \dot{Q}) = (\hat{w}, \hat{Q})e^{i(kx-\omega t)}, \qquad (6.5.7)$$

and substituting it into (6.5.6) yields

$$\frac{\partial^2 \hat{w}}{\partial z^2}+\left(\frac{N^2-\Omega^2}{\Omega^2-f^2}\right)k^2\hat{w}=\left(\frac{k^2}{\Omega^2-f^2}\right)\hat{Q}, \qquad (6.5.8)$$

where $\Omega = \omega - kU$ is the *Doppler-shifted frequency*. The above equation is similar to (3.6.8) except with the assumption of two-dimensionality and the addition of diabatic heating. Equation (6.5.8) contains a thermally forced mode and a free mode. Thus, as discussed in Chapter 3, the free mode includes the following three major flow regimes: (1) $\Omega > N > f$: *high-frequency evanescent flow regime*; (2) $N > \Omega > f$: *vertically propagating inertia-gravity wave regime*; and (3) $N > f > \Omega$: *low-frequency evanescent flow regime*. The disturbance decays exponentially with height and is confined to its neighborhood for evanescent flow regimes. It is able to propagate vertically as inertia-gravity waves for the vertically propagating inertia-gravity wave regime.

In applying (6.5.8) to sea breeze circulations with no basic wind ($U = 0$), the thermal forcing is controlled by the diurnal cycle of sensible heating, which has an intrinsic frequency (ω) of 7.272 x 10^{-5} s^{-1} ($= 2\pi/24\,\mathrm{h}$). Since ω is generally much smaller than N, (6.5.8) approximately reduces to

$$\frac{\partial^2 \hat{w}}{\partial z^2}+\left(\frac{N^2}{\omega^2-f^2}\right)k^2\hat{w}=\left(\frac{k^2}{\omega^2-f^2}\right)\hat{Q}, \qquad (6.5.9)$$

and only two flow regimes exist in the system, i.e. the vertically propagating inertia-gravity wave regime ($\omega > f$), and the low-frequency evanescent flow regime ($\omega < f$). In addition, the regime where $\omega = f$ should be considered (Rotunno 1983). In this particular flow regime, friction needs to be considered; otherwise (6.5.9) is singular.

This inviscid theory gives different flow regimes for latitudes higher and lower than 30°. In reality, however, the effects of friction and thermal diffusion influence the critical latitude that separates the vertically propagating inertia-gravity wave regime from the low-frequency evanescent flow regime. By prescribing the heating function as an arc tangent function and introducing a streamfunction ψ ($u' = \partial\psi/\partial z$; $w' = -\partial\psi/\partial x$), a mathematical problem similar to that governed by (6.5.9) has been solved analytically (Rotunno 1983). Figure 6.22 shows the

nondimensionalized horizontal velocity and vertical velocity fields for $f > \omega$. The horizontal scale of the sea breeze is confined within a distance of order $Nd/\sqrt{f^2-\omega^2}$, where *d* is the vertical scale of heating. When $f < \omega$, the response associated with the sea breeze circulations is in the form of inertia-gravity waves.

The above theory was extended to include Rayleigh friction [$(F_{r1}, F_{r2}, F_{r3}) = -\alpha(u', v', w')$] and Newtonian cooling ($\dot{Q} = -\alpha\theta'$). It is found (Dalu and Pielke 1989) that: (a) when friction is small, periodicity in the forcing enhances the intensity and the horizontal scale of the breeze; (b) when the friction e-folding time is of the order of one day, the opposite is true; (c) when the dissipation is small ($\alpha^2 < \omega^2 - f^2$), waves might occur after a few days of sea breeze below the latitude $\sin^{-1}\left(\sqrt{\omega^2-\alpha^2}/2\omega\right)$, which is lower than the 30° derived from inviscid theory; and (d) wave patterns below a latitude of 30° predicted by inviscid linear theory are likely to be rare.

Although friction controls the diffusion of momentum, it is not necessarily important for producing the sea breeze circulations (Niino 1987). Friction is important in satisfying the no-slip lower boundary condition at the ground level and producing a realistic wind profile near the ground. Thus, the vertical scale of the heating is a function of viscosity and cannot generally be prescribed as in the above linear theory. With the effects of friction included, it is found (Niino 1987) that: (a) the singularity at 30° latitude vanishes, (b) the horizontal extent of the sea breeze is controlled by $N\kappa^{1/2}\omega_*^{-3/2}g(f)$, where *N* is the buoyancy frequency, κ the eddy thermal diffusivity, ω_* the frequency of sea breeze toward the ground, and $g(f)$ is a universal function which remains constant (about 2.1) for latitudes below 30° and decreases rapidly to 0.9 at the North or the South Pole; and (c) nonhydrostatic effects are significant in the immediate neighborhood of the coastline. Sun and Orlanski (1981a, b) solved both linearized and nonlinear equations as initial values problems and confirmed that the two-day-waves can be easily excited by the diurnal oscillation of the land-sea contrast at lower latitudes (< 15 degrees). On the other hand, a combination of 1-day and 2-day waves may coexist up to 30 degrees. These waves may correspond to the mesoscale cloud bands observed along coastlines with a space interval of a few tens to few hundred kilometers.

6.5.2 Nonlinear numerical studies

Figure 6.23 shows an example of the structure of a sea breeze front, as simulated by a three-dimensional nonlinear numerical model. At 1000 local time (Fig. 6.23a), the sea breeze is about 400 m deep with a maximum horizontal velocity of about 6 ms^{-1} and a vertical velocity of about 1.5 ms^{-1} above the sea breeze front. The front has advanced a distance of about 6 km inland in spite of resistance from the offshore basic wind of 10 ms^{-1}. Since the sea breeze front has a scale of only 200 m, there is a need for treating it in greater detail. This is approached by utilizing higher horizontal resolution for more accurate and detailed simulation of the front. At 1200 local time (Fig. 6.23b), the sea breeze front advances to about 60 km inland and has developed to a depth of about 800 m. In three-dimensional simulations, *horizontal convective rolls* tend to develop over

land in response to strong daytime surface heating with a parallel alignment to the vertical wind shear vector (Dailey and Fovell 1999). The sea-breeze front, along with the horizontal convective rolls parallel to the front, are thus able to initiate deep convection (Fovell 2005).

At the nose of the sea breeze front, the denser sea breeze air overruns the less dense land airmass, an occurrence that extends to a height of approximately 100 m (Fig. 6.24). The sea-breeze front thus begins to behave like a density current. Its head is divided into a series of lobes and clefts. Some of the warmer air is overrun and ingested in the cleft in the center of the lobe, as depicted in Fig. 6.24. The spacing between the clefts is about 1 km. Longitudinal bands aligned with environmental shear vectors are the preferred mode of convection for small-amplitude perturbations over a flat terrain in both dry and saturated atmospheres, as revealed in theoretical studies (Asai 1972), although sometimes, the longitudinal band may coexist with transvers bands associated with gravity waves (Sun 1978). In addition to the sea-breeze front, *Kelvin-Helmholtz billows* have been observed; they are caused by the development of shear instability, as depicted in the schematic diagram of Fig. 6.25. These features of the sea-breeze front have also been reproduced in laboratory experiments.

Further advancement in numerical simulations of the sea and land breezes have been made by exploring the effects of diurnal variation, land breeze, isolated lakes and islands, basic wind shear, differences between land breeze and sea breeze, combined effects of sea breeze and mountain solenoidal circulations, initiation of and interaction with deep convection, air pollutant transport by sea-breezes, and mountain effects.

6.6 Dynamics of mountain-plains solenoidal circulations

- The dynamics of *mountain-plains solenoidal (MPS) circulations* is a little explored area of orographically influenced flow and weather phenomena. This is mainly due to the complicated interactions between orographic and thermal forcings.

- Taking into consideration sensible heating or cooling over elevated terrain results in a considerably more complex flow than has been considered until now. The classical view of orographically and thermally forced winds in mountains includes the slope and mountain-valley winds.

- During the day, the mountain serves as an elevated heat source due to the sensible heat released by the mountain surface.

  In a quiescent atmosphere, this can induce mountain *upslope flow or upslope wind*, which in turn may initiate cumuli or thunderstorms over the mountain peak and produce orographic precipitation.

- At night, the opposite occurs: surface cooling produces downslope *drainage flow*.

➢ Based on observations, four stages in the development of a thermally forced circulation generated by solar heating in a mountain valley have been identified (e.g., Banta 1990):

I. Before sunrise, the nocturnal inversion layer contains drainage flow, which generally blows in a different direction from the winds above the inversion. Just prior to sunrise, this very stable layer remains adjacent to the surface;
II. After sunrise, surface sensible heating erodes the inversion layer and produces a shallow *convective boundary layer* (*CBL*) below the inversion layer and the upslope flow;
III. The shallow CBL or upslope layer deepens as the surface heating continues; and
IV. After the nocturnal inversion layer disappears during the afternoon, a deep, well-mixed CBL is created.

Linear theories described in Sections 6.1 and 6.2 have been applied to study the combined effects of orographic and thermal forcing for mesoscale mountain flow (e.g., Raymond 1972; Smith and Lin 1982). Numerical modeling studies of the combined orographical and thermal forcing have been explored as early as the 1960's (e.g., Orville 1964, 1968). More sophisticated numerical models with a variety of initial conditions have been adopted in the more recent studies of mountain-plains solenoidal circulations. The results given by these models have been verified by conventional observations as well as field experiments (e.g. Tripoli and Cotton 1989; Wolyn and McKee 1994).

- Figure 6.26 shows a conceptual model for the daytime evolution of the MPS circulation.

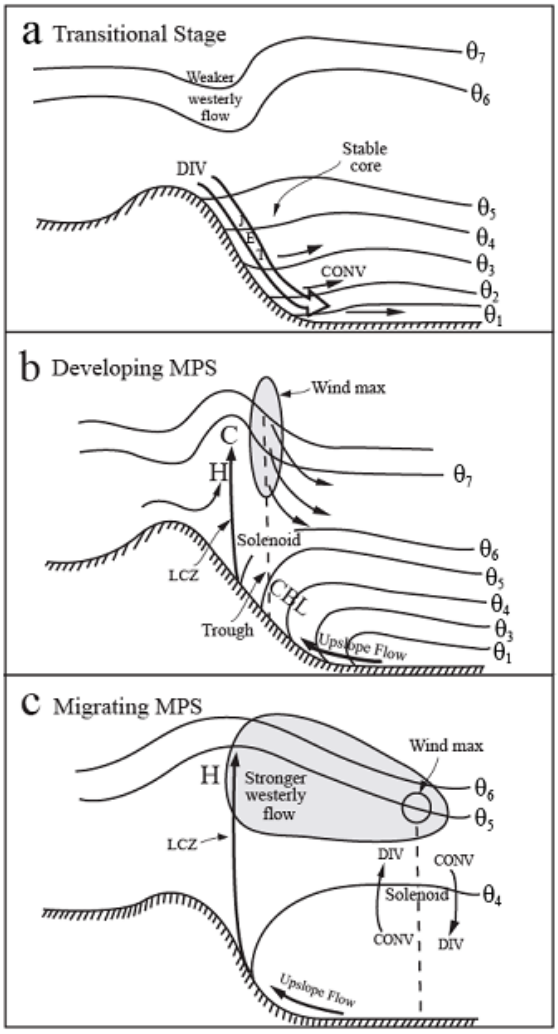

Fig. 6.26: Conceptual model of the daytime evolution of the mountain-plains solenoidal (MPS) circulation east of a mesoscale mountain under conditions of clear skies, steady-state synoptic-scale situation, and light basic westerly wind (e.g., 5 ms^{-1}). Three primary stages may be identified: (a) transition stage, (b) developing MPS stage, and (c) migrating MPS stage. Symbols DIV, CONV, JET, C, H, CBL, and LCZ denote divergence, convergence, katabatic jetlike flow, cold core, higher pressure, convective boundaru layer, and leeside convergence zone, respectively. Regions of wind maximum are shaded. Solid lines are the isentropes. (Adpated after Wolyn and McKee 1994)

The circulation primarily includes:

- Transitional stage
- Developing mountain-plain solenoidal (MPS) stage

- Migrating MPS stage.

The transitional stage occurs when the sun rises. The most pronounced feature of the transition stage is the katabatic jetlike flow down the east side of the mountain (Fig. 6.26a).

The slowing of the nocturnal jet on the eastern plains produces a convergence that lifts the cold air, thus creating a *stable core* that is shallower farther east of the barrier. This nocturnal katabatic flow weakens as it is affected by the surface heating, and is replaced by a mesoscale solenoidal circulation 3-4 h after sunrise (Fig. 6.26b).

A shallow convective boundary layer (CBL) is produced below the inversion layer and an upslope flow is produced by the horizontal pressure gradient force toward the slope in response to the buoyancy associated with the surface sensible heating. The main upward motion of the solenoidal circulation occurs in a narrow zone over the eastern slope of the mountain, and is called the *leeside convergence zone* (LCZ). The LCZ lifts the air into the ambient air above, creating the cold core (denoted by "C" in Fig. 6.26b).
A strong sinking motion occurs to the east of the cold core, creating a pressure trough in which the center of the solenoid is located. The horizontal pressure gradient associated with the cold core and the trough to the east produces a horizontal

wind speed maximum. A broad region of sinking motion is located to the east of the solenoid center.

At the later time of this stage, the sinking and horizontal warm-air advection immediately east of the solenoid center is able to warm the air enough to create a negative pressure gradient in the stable core above the CBL.

The final stage of the mountain-plains solenoidal circulation is characterized by the eastward migration (Fig. 6.26c). Convergence (divergence) near the height of the wind maximum region and divergence (convergence) near the surface tend to produce sinking motion ahead (behind) the horizontal wind maximum located beneath the leading edge of the cold core,.

The solenoid center is located in a pressure trough beneath the eastward-moving leading edge of the cold core, while the LCZ remains anchored over the lee slopes. Only the migrating MPS may be defined as a disturbance, and as thus can significantly affect the atmosphere on the plains located east of the system during the daytime circulations. The CBL grows explosively and the depth of the upslope flow increases when the solenoid passes a location.

The MPS has been shown to be responsible for producing a strong updraft, which in turn generated the dominant wave of the second episode of gravity waves observed on 11-12 July 1981 during the Cooperative Convective Precipitation Experiment (Koch et al. 2001). A

gravity wave was generated as the updraft impinged upon a stratified shear layer above the deep, well-mixed boundary layer developed by strong sensible heating over the Absaroka Mountains. Explosive convection developed directly over the remnant gravity wave as an eastward-propagating density current, produced by a rainband generated within the MPS leeside convergence zone, merged with a westward-propagating density current in eastern Montana. The complicated interactions of differing sensible heat contributions from complex terrain, gravity waves, and convection indicate the need for increasingly detailed observations and theories to verify existing MPS hypotheses and gravity wave generation.

Appendix 6.1: Laplace transform

If a function *f*(*t*) is defined in the interval $0 \le t < \infty$, where t and f(t) are real, then the function $\hat{f}(s)$, defined by the *Laplace integral*

$$\hat{f}(s) = \mathcal{L}(f(t)) = \int_0^\infty f(t)e^{-st}dt, \qquad \text{(A6.1.1)}$$

where *s* is a complex number. The transformation of *f*(*t*) into $\hat{f}(s)$ is called the *Laplace transform*, which is often used to solve differential equations involving time. The first step is to apply (A6.1.1) to transform the differential equation into the Laplace space. The second is to find the solution for the unknown function $\hat{f}(s)$ in the Laplace space. The third step is to invert $\hat{f}(s)$ back to the physical space *f*(*t*), i.e., to take the *inverse Laplace transform*. The actual inverse Laplace transform involves the contour integration in the complex plane, but in practice it is often performed by applying some known properties of Laplace transform, such as the linear property,

$$\mathcal{L}(af(t) + bg(t)) = a\hat{f}(s) + b\hat{g}(s)$$

. (A6.1.2)

Some basic properties of Laplace transform and inverse Laplace transform can be found in Hildebrand (1976), among other mathematical textbooks.

References

Adler, R. F., and R. A. Mack, 1986: Thunderstorm cloud top dynamics inferred from satellite observations and a cloud top parcel model. *J. Atmos. Sci.*, **43**, 1945-1960.

Asai, T., 1972: Thermal instability of a shear flow turning the direction with height. *J. Meteor. Soc. Japan*, **50**, 525-532.

Baik, J.-J., and H.-Y. Chun, 1997: A dynamical model for urban heat islands. *Bound.-Layer Meteor.*, **83**, 463-477.

Baik, J.-J., H.-S. Hwang, and H.-Y. Chun, 1999: Transient, linear dynamics of a stably stratified shear flow with thermall forcing and a critical level. *J. Atmos. Sci*., **56**, 483-499.

Banta, R. M., 1990: The role of mountain flows in making clouds. *Atmospheric Processes over Complex Terrain*, *Meteor. Monogr.*, **45**, Amer. Meteor. Soc., 229-283.

Bretherton, C., 1988: Group velocity and the linear response of stratified fluids to internal heat or mass sources. *J. Atmos. Sci.*, **45**, 81-93.

Bretherton, C., 1993: The nature of adjustment in cumulus cloud fields. *The Representation of Cumulus Convection in Numerical Models*, *Meteor. Monogr*., **46**, Amer. Meteor. Soc., 63-74.

Chun, H.-Y., and J.-J. Baik, 1994: Weakly nonlinear response of a stably stratified atmosphere to diabatic focing in a uniform flow. *J. Atmos. Sci.*, **51**, 3109-3121.

Chun, H.-Y., and Y.-L. Lin, 1995: Enhanced response of an atmospheric flow to a line type heat sink in the presence of a critical level. *Meteor. Atmos. Phys.*, **55**, 33-45.

Crook, N. A., and M. W. Moncrieff, 1988: The effect of large-scale convergence on the generation and maintenance of deep moist convection. *J. Atmos. Sci.*, **45**, 3606-3624.

Dailey, P. S., and R. G. Fovell, 1999: Numerical simulation of the interaction between the sea-breeze front and horizontal convective rolls. Part I: Offshore ambient flow. *Mon. Wea. Rev.*, **127**, 858-878.

Dalu, G. A., and R. A. Pielke, 1989: An analytical study of the sea breeze. *J. Atmos. Sci.*, **46**, 1815-1825.

Doyle, J. D., and T. T. Warner, 1993: Nonhydrostatic simulations of coastal mesoscale vortices and frontogenesis. *Mon. Wea. Rev.*, **121**, 3371-3392.

Fovell, R. G. 2005: Convective initiation ahead of the sea-breeze front. *Mon. Wea. Rev.*, **133**, 264-278.

Garstang, M., P. D. Tyson, and G. D. Emmitt, 1975: The structure of heat islands. *Rev. Geophys. Space Phys.*, **13**, 139-165.

Heymsfield, G. M., and R. H. Blackmer, Jr., 1988: Satellite-observed characteristics of Midwest severe thunderstorm anvils. *Mon. Wea. Rev.*, **116**, 2200-2224.

Hildebrand, F. B., 1976: *Advanced Calculus for Applications*. 2nd Ed., Prentice-Hall Inc., USA, 733pp.

Hjelmfelt, M. R., 1982: Numerical simulations of the effects of St. Louis on mesoscale boundary layer airflow and vertical air motion: Simulations of urban vs non-urban effects. *J. Appl. Meteor.*, **31**, 1239-1257.

Hsu, H.-M., 1987: Mesoscale lake-effect snowstorms in the vicinity of Lake Michigan: Linear theory and numerical simulations. *J. Atmos. Sci.*, **44**, 1019-1040.

Kimura, R., and T. Eguchi, 1978: On dynamical processes of sea- and land-breeze circulation. *J. Meteor. Soc. Japan*, **56**, 67-85.

Koch, S. E., F. Zhang, M. L. Kaplan, Y.-L. Lin, R. P. Weglarz, and C. M. Trexler, 2001: Numerical simulations of a gravity wave event over CCOPE. Part III: The role of a mountain-plains solenoid in the generation of the second wave episode. *Mon. Wea. Rev.*, **129**, 909-933.

Lin, C. A., and R. E. Stewart, 1991: Diabatically forced mesoscale circulations in the atmosphere. *Adv. Geophys.*, **33**, B. Saltzman (Ed.), Academic Press, NY, 267-305.

Lin, Y.-L., 1986: Calculation of airflow over an isolated heat source with application to the dynamics of V-shaped clouds. *J. Atmos. Sci.*, **43**, 2736-2751.

Lin, Y.-L., 1987: Two-dimensional response of a stably stratified flow to diabatic heating. J. Atmos. Sci., 44, 1375-1393.

Lin, Y.-L., 1989: Inertial and frictional effects on stratified hydrostatic airflow past an isolated heat source. *J. Atmos. Sci.*, **46**, 921-936.

Lin, Y.-L., 1990: A theory of cyclogenesis forced by diabatic heating. Part II: A semi-geostrophic approach. *J. Atmos. Sci.*, **47**, 1755-1777.

Lin, Y.-L., 1996: Structure of dynamically unstable shear flow and their implications for shallow internal gravity waves. Part II: Nonlinear response. *Meteor. Atmos. Phys.*, **59**, 153-172.

Lin, Y.-L., and H.-Y. Chun, 1991: Effects of diabatic cooling in a shear flow with a critical level. *J. Atmos. Sci.*, **48**, 2476-2491.

Lin, Y.-L., and S. Li, 1988: Three-dimensional response of a shear flow to elevated heating. *J. Atmos. Sci.*, **45**, 2987-3002.

Lin, Y.-L., and R. B. Smith, 1986: Transient dynamics of airflow near a local heat source. *J. Atmos. Sci.*, **43**, 40-49.

Lin, Y.-L., T.-A. Wang, and R. P. Weglarz, 1993: Interaction between gravity waves and cold air outflows in a stably stratified uniform flow. *J. Atmos. Sci.*, **50**, 3790-3816.

Lyons, W. A., and L. E. Olsson, 1972: The climatology and prediction of the Chicago lake breeze. *J. Appl. Meteor.*, **11**, 1254-1272.

Nicholls, M. E., R. A. Pielke, and W. R. Cotton, 1991: Thermally forced gravity waves in an atmosphere at rest. *J. Atmos. Sci.*, **48**, 1869-1884.

Niino, H., 1987: The linear theory of land and sea breeze circulation. *J. Meteor. Soc. Japan*, **65**, 901-921.

Ogura, Y., and M.-T. Liou, 1980: The structure of a midlatitude squall line: A case study. *J. Atmos. Sci.*, **37**, 553-567.

Olfe, D. B., and R. L. Lee, 1971: Linearized calculation of urban heat island convection effects. *J. Atmos. Sci.*, **28**, 1374-1388.

Orville, H. D., 1964: On mountain upslope winds. *J. Atmos. Sci.*, **21**, 622-633.

Orville, H. D., 1968: Ambient wind effects on the initiation and development of cumulus clouds over mountains. *J. Atmos. Sci.*, **25**, 385-403.

Raymond, D. J., 1972: Calculation of airflow over an arbitrary ridge including diabatic heating and cooling. *J. Atmos. Sci.*, **29**, 837-843.

Raymond, D. J., and R. Rotunno, 1989: Response of a stably stratified flow to cooling. *J. Atmos. Sci.*, **46**, 2830-2837.

Reuter, G. W., and O. Jacobsen, 1993: Effects of variable wind shear on the mesoscale circulation forced by slab-symmetric diabatic heating. *Atmosphere-Ocean*, **31**, 451-469.

Riordan, A. J., 1990: Examination of the mesoscale features of the GALE coastal front of 24-25 January 1986. *Mon. Wea. Rev.*, **118**, 258-282.

Riordan, A. J., and Y.-L. Lin, 1992: Mesoscale wind signatures along the Carolina coast. *Mon. Wea. Rev.*, **120**, 2786-2797.

Robichaud, A., and C. A. Lin, 1989: Simple models of diabatically forced mesoscale circulations and a mechanism for amplification. *J. Geophys. Res.*, **94**, D3, 3413-3426.

Rotunno, R., 1983: On the linear theory of the land and sea breeze. *J. Atmos. Sci.*, **40**, 1999-2009.

Schmidt, J. M., and W. R. Cotton, 1990: Interactions between upper and lowetr atmospheric gravity waves on squall line structure and maintenance. *J. Atmos. Sci.*, **47**, 1205-1222.

Simpson, J. E., 1994: *Sea Breeze and Local Winds*. Cambridge University Press, 234pp.

Smith, R. B., 1980: Linear theory of stratified hydrostatic flow past an isolated mountain. *Tellus*, **32**, 348-364.

Smith, R. B., and Y.-L. Lin, 1982: The addition of heat to a stratified airstream with application to the dynamics of orographic rain. *Quart. J. Roy. Meteor. Soc.*, **108**, 353-378.

Song, I.-S., and H.-Y. Chun, 2005: Momentum flux spectrum of convectively forced internal gravity waves and its application to gravity wave drag parameterization. Part I: Theory. *J. Atmos. Sci.*, **62**, 107-124.

Sousounis, P. J., and H. N. Shirer, 1992: Lake aggregate mesoscale disturbances. Part I: Linear analysis. *J. Atmos. Sci.*, **49**, 80-96.

Sun, W.-Y., 1978: Stability analysis of cloud streets. *J. Atmos. Sci.*, **35**, 466-483.

Sun, W.-Y., and I. Orlanski, 1981a: Large mesoscale convection and sea breeze circulation. Part I: Linear stability analysis. *J. Atmos. Sci*., **38**, 1675-1693.

Sun, W.-Y., and I. Orlanski, 1981b: Large mesoscale convection and sea breeze circulation. Part 2: Non-Linear numerical model. *J. Atmos. Sci.*, **38**, 1694-1706.

Szeto, K. K., C. A. Lin, and R. E. Steward, 1988: Mesoscale circulations forced by melting snow. II: Application to meteorological features. *J. Atmos. Sci.*, **45**, 1642-1650.

Thorpe, A. J., M. J. Miller, and M. W. Moncrieff, 1980: Dynamical models of two-dimensional downdraughts. *Quart. J. Roy. Meteor. Soc.*, **106**, 463-484.

Tripoli, G. J., and W. R. Cotton, 1989: Numerical study of an observed mesoscale convective system. Part I: Simulated genesis and comparison with observations. *Mon. Wea. Rev.*, **117**, 273-304.

Wang, P. K., 2003: Moisture plumes above thunderstorm anvils and their contributions to cross-tropopause transport of water vapor in midlatitudes. *J. Geophys. Res.*, **108,** D6, 4194-4208.

Wolyn, P. G., and T. B. McKee, 1994: The mountain-plains circulation east of a 2-km-high north-south barrier. *Mon. Wea. Rev.*, **122**, 1490-1508.

Xie, L., and Y.-L. Lin, 1996: Responses of low-level flow to an elongated surface heat source with application to coastal frontogenesis. *Mon. Wea. Rev.*, **124**, 2807-2827.